Arabian Journal of Chemistry (2017) xxx, xxx–xxx

King Saud University

Arabian Journal of Chemistry

www.ksu.edu.sa
www.sciencedirect.com

Design and nonlinear optical properties (NLO) using DFT approach of new Cr(III), VO(II), and Ni(II) chelates incorporating tri-dentate imine ligand for DNA interaction, antimicrobial, anticancer activities and molecular docking studies

Laila H. Abdel-Rahman [a], **Ahmed M. Abu-Dief** [a,*], **H. Moustafa** [b], **Azza A. Hassan Abdel-Mawgoud** [a]

[a] *Chemistry Department, Faculty of Science, Sohag University, 82524, Egypt*
[b] *Chemistry Department, Faculty of Science, Cairo University, 12613 Giza, Egypt*

Received 12 May 2017; accepted 12 July 2017

KEYWORDS

Imine complexes;
Nonlinear optical properties (NLO);
DFT calculations;
Antimicrobial activity;
DNA interaction;
Anticancer

Abstract In recent years, metals based antitumor complexes have played a vital role in chemotherapy. Therefore, in this study, some new imine Cr(III), VO(II) and Ni(II) complexes incorporating ESAP imine ligand (2-Ethoxy-6-((2-hydroxy-phenylimino)-methyl)-phenol were designed and synthesized. The investigated complexes were fully characterized by micro analysis, infrared, electronic spectra, thermal analysis (TGA), conductivity as well as magnetic susceptibility measurements. Moreover, the stability constants of the prepared complexes were determined spectrophotometrically. The results suggest that the titled ESAP imine ligand serves as tri-dentate moiety through deprotonated two phenolic oxygen and azomethene nitrogen atoms for coordination to Cr(III) in octahedral geometry, tetrahedral to Ni(II) and distorted square pyramidal to VO(II). The electronic structure and nonlinear optical parameters NLO of the newly synthesized complexes are investigated theoretically at the B3LYP/GEN level of theory. The studied complexes show promising optical properties. Indeed, the prepared compounds were evaluated for antimicrobial effect against some types of bacteria and fungi. The investigated complexes exhibit a stronger antimicrobial efficiency compared to its ligand. Moreover, the interaction of the complexes with CT-DNA was monitored using spectral studies, viscosity and gel electrophoreses measurements. Furthermore, the cytotoxic activity of the prepared imine complexes on human colon carcinoma cells, hepatic cellular

* Corresponding author.
E-mail address: ahmed_benzoic@yahho.com (A.M. Abu-Dief).
Peer review under responsibility of King Saud University.

Production and hosting by Elsevier

http://dx.doi.org/10.1016/j.arabjc.2017.07.007

Please cite this article in press as: Abdel-Rahman, L.H. et al., Design and nonlinear optical properties (NLO) using DFT approach of new Cr(III), VO(II), and Ni(II) chelates incorporating tri-dentate imine ligand for DNA interaction, antimicrobial, anticancer activities and molecular docking studies. Arabian Journal of Chemistry (2017), http://dx.doi.org/10.1016/j.arabjc.2017.07.007

carcinoma cells and breast carcinoma cells have shown promising results and enhancement of the anti-proliferative activity compared to its ligand. The molecular docking into TRK (PDB: 1t46) was done for the optimization of the investigated compounds as potential TRK inhibitors.

1. Introduction

Study of coordination chemistry of transition metal ions with different kinds of ligands has been enhanced by the current advancements in the fields of bioinorganic chemistry, the design of molecular ferromagnets, liquid crystals (Canali and Sherrington, 1999; Lin et al., 2003; Abu-Dief and Mohamed, 2015), medical imaging (Lacroix, 2001) and optical materials (Abu-Dief et al., 2013). Through the years, imines have played a special role as chelating ligands in main group and transition metal coordination chemistry, as their stability under a variety of oxidative and reductive conditions, and to the fact that imine ligands are borderline between hard and soft Lewis bases (Hosseini-Yazdi et al., 2014; Anacona and Santaella, 2013; Abdel-Rahman et al., 2014a). Metal coordination compounds have wide assorted qualities of technological and modern applications ranging from catalysis to anti-tumor drugs. This is may be due to the complexes containing oxygen and nitrogen atoms go about as models for metalloproteins, metalloenzymes which catalyze the reduction of nitrogen and oxygen (Ziessel, 2001). In the literature, there is no systematic study of the electronic structure and nonlinear properties of the studied complexes. Such study is important for understanding the electronic structure, biological activity and NLO properties of these complexes. In recent years, a large number of research have been performed to examine different various of nonlinear optical (NLO) materials (Wojciechowski et al., 2010) in order to design excellent NLO materials which indicate potential application in modern communication technology, data storage and optical signal processing (Marder et al., 1991). The microscopic structure-property relationship for such complexes may lead to discovery of improved NLO characteristics material, thus, facilitating the design of new molecules for potential NLO applications. This could be made through study of response electric properties, namely, polarizability, hyperpolarizability of the molecules using computational methods. One of the nonlinear optical phenomena is the second harmonic generation (SHG) where intense light of longer wave length is changed to half of the incident value, upon absorption by the nonlinear optical material.

On the other hand, cancer is one of the most widespread deadly diseases and poses serious challenges for the medical community; it takes third place among causes of mortality in the human population throughout the world.

From this point of view and continuation of our previous work (Abu-Dief et al., 2015; Abu-Dief and Nassr, 2015; Abdel-Rahman et al., 2013a,b; 2014a,b,c; 2015a,b; 2016a,b,c,d,e,f; 2017a,b,c,d,e,f,g), in the present study, we found it is worth to synthesis of new tridentate Cr(III), VO(II) and Ni(II) imine complexes. The spectral and thermal properties of these complexes were studied in details. Also the kinetic parameters for decomposition steps in thermograms of these complexes were calculated. Moreover, the geometrical parameters (bond lengths, bond angles and dihedral angles), NBO analysis (natural charges, natural population and natural configuration) and electrostatic potential of the studied complexes were calculated using B3LYP/GEN. The electronic dipole moment (μ) and first order hyperpolarizibility (β) values of the studied complexes have been computed to study the NLO properties. Global reactivity descriptors; electronegativity (X), hardness (η), softness (S) of the studied complexes were calculated and analyzed. In addition to, the biological activity of the investigated ESAP ligand and its complexes was studied against selected kinds of bacteria and fungi. Moreover, the interaction of the complexes with Calf thymus DNA (CT-DNA) was studied. Furthermore, the cytotoxic activities of the prepared imine complexes against different cancer cell lines were evaluated.

2. Experimental

2.1. Reagents

All of the reagents and solvents used for synthesis were of commercially available reagent grade and utilized without purification. They included 3-ethoxysalicyldehyde, 2-amino phenol, vanadyl acetylacetonate ($VO(C_5H_7O_2)_2$), chromium nitrate ($Cr(NO_3)_3{\cdot}6H_2O$) and nickel nitrate ($Ni(NO_3)_2{\cdot}6H_2O$) were obtained from Sigma-Aldrich. Spectroscopic grade ethanol, dimethylformamide (DMF) and HCl products were used.

Calf thymus DNA(CT-DNA), bromophenol blue dye, ethidium bromide and Tris(hydroxymethyl)-aminomethane(Tris) were acquired from (Sigma-Aldrich Chemie (Germany)).

2.2. Preparation of ESAP imine ligand2.2

5 mmole (0.83 g) of 3-ethoxysalicyldehyde was dissolved in ethanol and mixed with ethanolic solution of 5 mmole (0.545 g) of 2-amino phenol. Then the mixture was refluxed and stirred for 2 h at 90 °C and the orange precipitate was formed. The product separated was filtered, washed with ethanol and dried over anhydrous $CaCl_2$.

^{1}H NMR (δ, ppm), in DMSO-d_6: δ = 1.36 (d, ^3J = 5.1 Hz, 3H, CH_3), 4.09 (d, ^3J = 7.8 Hz, 2H, CH_2), 6.84 (t, ^3J = 7.8 Hz, 1H, H-4), 6.89 (t, ^3J = 7.9, 8.2 Hz, 1H, H-5′), 6.98 (d, ^3J = 8.1 Hz, 1H, H-3′), 7.07 (d, ^3J = 8.0 Hz, 1H, H-3), 7.13 (t, ^3J = 7.9 Hz, 1H, H-4′), 7.19 (d, ^3J = 7.8 Hz, 1H, H-5), 7.36 (d, ^3J = 8.0 Hz, 1H, H-6′), 8.94 (s, 1H, CH═N), 9.61 (s, 1H, 1-OH), 13.90 ppm (s, 1H, 2′-OH).

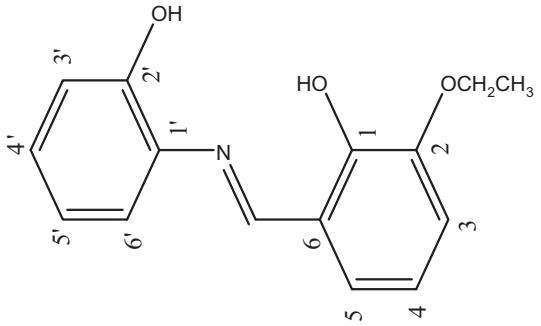

^{13}C NMR (δ, ppm), in DMSO-d_6: δ = 15.2 (CH, CH_3), 64.7 (CH, CH_2), 117.0 (CH), 117.6 (CH), 118.4 (CH), 120.1 (CH), 124.5 (CH), 128.3 (CH), 128.6 (C_q), 135.1 (C_q), 147.7 (C_q), 151.4 (CH), 152.7 (C_q), 154.9 (C_q), 162.1 ppm (CH═N).

Please cite this article in press as: Abdel-Rahman, L.H. et al., Design and nonlinear optical properties (NLO) using DFT approach of new Cr(III), VO(II), and Ni(II) chelates incorporating tri-dentate imine ligand for DNA interaction, antimicrobial, anticancer activities and molecular docking studies. Arabian Journal of Chemistry (2017), http://dx.doi.org/10.1016/j.arabjc.2017.07.007

2.3. Preparation of ESAPCr, ESAPNi and ESAPV complexes

Cr(III), VO(II) and Ni(II) imine complexes were obtained according to a general procedure: 10 mmole (2.57 g) of ESAP ligand was dissolved in ethanol with yellow color and 10 mmole of metal salt (4.00 g of Cr^{3+}, 2.98 Ni^{2+} or 2.65 (VO^{2+})) was dissolved in aqueous-ethanolic mixture. The two solutions were mixed together and refluxed for 2 h at 85 °C. The solid product obtained on cooling was filtered, washed several time with hot water followed by ethanol and diethyl ether. Finally, all the prepared complexes were dried at room temperature over $CaCl_2$.

2.4. Analytical and physical measurements

Melting point for the titled ESAP imine ligand and decomposition temperatures for its prepared complexes were carried out on a melting point device, Gallenkamp, UK. Infrared spectra were recorded as KBr pellets using Shimadzu. FTIR-8300 spectrophotometer. ^{1}H and ^{13}C NMR spectra were obtained in DMSO-d_6 solutions with a Bruker Avance DPX-500 spectrometer. All of the scanning UV–Vis spectra in DMF were registered using 10 mm matched quartz cells through PG spectrophotometer model T + 80. Elemental analyses which were made at main lab of Cairo University by Elemental analyzer Perkin-Elmer (model240c). The instrument employed for recording magnetic susceptibility were performed on Gouy's balance and the diamagnetic corrections were executed by Pascal's constants. Thermo gravimetric check was made under nitrogen with a heating rate 10 °C min^{-1} on Shimaduz corporation 60H analyzer. The values of absorbance of 5×10^{-3} M of each complex were measured at various pH levels. The pH levels were tested by using a series of Britton universal buffers (Abdel-Rahman et al., 2013a,b; 2014a,c; 2015a,b; 2016a,b,c; 2017b,c,d,e,f,g). A HANNA 211 pH meter at 298 K equipped with a CL-51B combined electrode was utilized to pH measurements, calibrated against standard buffers (pH 4.02 and 9.18) before measurements.

2.5. Evaluation of the stoichiometry of the prepared imine complexes

The molar ratio (Abdel-Rahman et al., 2013a,b; 2015a,b; 2016a,b,c,d,e,f; 2017b,c,d,e,f,g) and continuous variation methods (Abd El-Lateef et al., 2015a,b; 2017) were used to study the equilibria in solutions and to determine M:L ratio.

2.6. Evaluation of the apparent formation constants of the synthesized complexes

The formation constants (K_f) of the studied imine complexes formed in solutions were obtained from the spectrophotometric measurements by using the continuous variation method (Abdel-Rahman et al., 2013a,b; 2014a; 2015a,b; 2016a,b,c,d,e,f; 2017b,c,d,e,f,g) according to the following relation.

$$K_f = \frac{A/A_m}{(1 - A/A_m)^2 C}$$

where A_m is the absorbance at the maximum formation of the complex, A is the arbitrary chosen absorbance values on either side of the absorbance mountain col (pass) and C is the initial concentration of the metal. Also, the free energy change, $\Delta(G^*)$ of the complexes was determined by $\Delta(G^*) = -RT \ln K_f$, at 25 °C where K_f, is the formation constant, R is the gas constant and T is the temperature in Kelvin.

2.7. Kinetic studies

The kinetic parameters of decomposition process for metal complexes were extracted from Coast-Redfern integral method (Abdel-Rahman et al., 2015b; 2016b,c; 2017b). The thermodynamic parameters such as the energy of activation (E^*) the entropy of activation (ΔS^*), enthalpy (ΔH^*) and free energy change (ΔG^*) of the decomposition of the metal complexes by employing the following equation,

$$\log\left[\frac{\log(w_\infty/(w_\infty - w))}{T^2}\right] = \log\left[\frac{AR}{\phi E^*}\left(1 - \frac{2RT}{E^*}\right)\right] - \frac{E^*}{2.303RT} \quad (1)$$

where w_∞ is the mass loss at the completion of the decomposition reaction, w is the mass loss over temperature T, R is the universal gas constant and ϕ is the heating rate. Since $1 - 2RT/E^* \approx 1$. A plot of the left-hand side of Eq. (1) against 1/T gives a slope from which E^* was calculated and A was determined from the intercept. The other kinetic parameters; the entropy of activation (ΔS^*), enthalpy of activation (ΔH^*) and the free energy change of activation (ΔG^*) were calculated using the following expression (Abdel-Rahman et al., 2015b; 2016b,c; 2017b–g):

$$\Delta S^* = 2.303R \log \frac{Ah}{K_B T} \quad (2)$$

$$\Delta H^* = E^* - RT \quad (3)$$

$$\Delta G^* = H^* - T\Delta S^* \quad (4)$$

where (K_B) and (h) are Boltzmann's and Plank's constants, respectively.

2.8. Computational methods for confirmation the proposed structures of the prepared complexes

All computations were carried out utilizing Gaussian 09W software package (Frisch et al., 2009). Molecular geometries of all the studied metal chelates were completely optimized using B3LYP/LANL2DZ (Schaefer et al., 1982; Becke, 1993). No symmetry constrains were applied through the geometry optimization (Reed and Weinhold, 1983). By using HOMO and LUMO energy values for complexes, electronegativity and chemical hardness can be calculated as follows: $X = (I + A)/2$ (electronegativity), $\eta = (I - A)/2$ (chemical hardness), $S = 1/2\eta$ (chemical softness) where I and A are ionization potential and electron affinity, and $I = -E_{HOMO}$ and $A = -E_{LUMO}$, respectively (Chandra and Uchimara, 2001). NBO calculations have been studied at the B3LYP/LANL2DZ level using NBO 3.1 program as performed in the Gaussian 09W software package in order that qualitatively measure the intermolecular delocalization in the studied complexes. Throughout this work, MOs were arranged using the Gauss-view 5.08 visualization program (Chen et al., 2009). The total

Please cite this article in press as: Abdel-Rahman, L.H. et al., Design and nonlinear optical properties (NLO) using DFT approach of new Cr(III), VO(II), and Ni(II) chelates incorporating tri-dentate imine ligand for DNA interaction, antimicrobial, anticancer activities and molecular docking studies. Arabian Journal of Chemistry (2017), http://dx.doi.org/10.1016/j.arabjc.2017.07.007

static dipole moment (μ), the mean polarizability ⟨α⟩, the anisotropy of the polarizability Δα and the mean first hyperpolarizability ⟨β⟩ using the x, y, z components were calculated by utilizing the following equations (Avci et al., 2010; Avci, 2011):

$$\mu = \left(\mu_x^2 + \mu_y^2 + \mu_z^2\right)^{1/2} \quad (5)$$

$$\alpha = \frac{(\alpha_{xx} + \alpha_{yy} + \alpha_{zz})}{3} \quad (6)$$

$$\Delta\alpha = ((\alpha_{xx} - \alpha_{yy})^2 + (\alpha_{yy} - \alpha_{zz})^2 + (\alpha_{zz} - \alpha_{xx})^2/2)^{1/2}, \quad (7)$$

$$\langle\beta\rangle = (\beta_x^2 + \beta_y^2\beta_z^2)^{1/2} \quad (8)$$

where

$$\beta_x = \beta_{xxx} + \beta_{xyy} + \beta_{xzz} \quad (9)$$

$$\beta_y = \beta_{yyy} + \beta_{xxy} + \beta_{yzz} \quad (10)$$

$$\beta_z = \beta_{zzz} + \beta_{xxz} + \beta_{yyz} \quad (11)$$

2.9. Antimicrobial efficiencies

The *in vitro* biological efficiency of the investigated ESAP imine ligand and its metal were screened against various types of bacteria (*Bacillussubtilis* (+*ve*), *Escherichia coli* (−*ve*) and *chelates Staphylococcusaureus* (+*ve*)) by well diffusion method utilizing nutrient agar as the environment (Abdel-Rahman et al., 2013; 2015a,b; 2016a,b,c; 2017a,b,c,d,e,f,g). The antifungal actions of the compounds were also investigated by the well diffusion method against various kinds of fungi (*Asperagillusniger*, *Candidaglabrata* and *Trichophyton rubrum*) on potato dextrose agar as circumference. The metal chelates have been dissolved in dimethylsulphoxide and the concentrations of the solutions are 10,000 and 20,000 ppm were set up separately. In a typical method, a well was made on the agar medium inoculated with micro-organism (Abdel-Rahman et al., 2013b; 2014a; 2015a,b; 2016a,b,c; 2017a,b,c,d,e). The well was full of the check solution using a micropipette and the plate was incubated 24 h at 37 °C for the bacteria or 72 h at 35 °C for the fungi. After incubation, the diameter of the obvious zone of inhibition around the sample was taken as a criterion for the inhibitory power of the sample against the specific check organism. The first tube without turbidity was considered as the MIC. Gentamycin was presented as positive standard for bacteria and Fluconazol was presented as positive standard for fungi. The sensitivity was registered by measuring the clear zone of growth inhibition of agar surface around the well in millimeter. to illustrate the impact of solvent (DMSO) on the biological screening, DMSO alone was presented as blank, and it showed no efficiency against microbial strains. The measurements were performed in triplicate for each compound and their average values are evaluated.

2.10. DNA binding propensity

All the tests including the interaction of the investigated metal imine chelates with DNA were performed in Tris–HCl buffer (60 mM, pH7.1). CT-DNA was purified by centrifugal dialysis previously utilize. A solution of calf thymus DNA in the buffer presented a proportion of UV absorption at 260 and 280 nm of about >1.85, show that the DNA was sufficiently free from protein contamination (12–18). The concentration of DNA was evaluated by monitoring the UV absorbance at 260 nm utilizing ε_{260} = 6600 mol^{-1} cm^2. The stock solution was conserved at 4 °C and utilized within only one day.

2.10.1. Electronic spectra for interaction of the prepared complexes with DNA

Spectrophotometric scan test was carried out by conservation the molar concentration of the investigated metal imine chelates constant while change the (DNA) in the surrounding conditions. The absorption due to free CT-DNA was removed by accession an equimolar CT-DNA to refine buffer solution in the blank compartment and the forming spectra were considered to result from the complexes and the DNA – metal complex assemblages (Abdel-Rahman et al., 2013a,b; 2014a; 2015a,b; 2016a,b,c; 2017a,b,c,d,e,f,g). From the absorption data, the intrinsic binding invariable (K_b) was determined by plotting (DNA)/(ε_a-ε_f) vs. (DNA) according to the following equation:

$$\frac{[DNA]}{(\varepsilon_a - \varepsilon_f)} = \frac{[DNA]}{(\varepsilon_b - \varepsilon_f)} + \frac{1}{[K_b(\varepsilon_b - \varepsilon_f)]} \quad (12)$$

where (DNA) is the concentration of DNA in base pairs, ε_a, ε_f and ε_b are the apparent, free and fully bound complex extinction coefficients, respectively. In particular, ε_f was evaluated from the calibration curve of the isolated metal complex; verifying the Beer's law. ε_a was evaluated as the ratio between the determined absorbance and the M(II) complex concentration, A_{obs}/(complex). The data were suitable for the above equation with a slope equal to 1/(ε_b-ε_f) and y-intercept equal to 1/(K_b(ε_b-ε_f)) and K_b was obtained from the ratio of slope to intercept. The standard Gibbs free energy for DNA binding was estimated from the following relation (Abdel-Rahman et al., 2013; 2015a,b; 2016a–c; 2017a–g):

$$\Delta G_b^{\neq} = -RT \ln K_b \quad (13)$$

2.10.2. Hydrodynamic measurements

Hydrodynamic measurements were performed utilizing an Oswald micro viscometer, keeped at constant temperature at 25 °C. The fluidity times were recorded for various concentrations of the complex (5–50 μM), maintaining the concentration of DNA constant (260 μM). Mixing of the solution was achieved by bubbling the nitrogen gas through the viscometer. The mean value of the three measures was utilized for determining the viscosity of the samples. The buffer fluidity time in seconds was recorded as t°. The relative viscosities for DNA in the presence (η) and absence (η°) of the complex were evaluated utilizing the relation η = (t − t°)/t°. Where, t is the recorded fluidity time in seconds and the amounts of the relative viscosity (η/η°) were plotted against 1/R (R = (DNA)/(Complex)) (Abdel-Rahman et al., 2013a,b; 2014a; 2015a,b; 2016a–c, 2017a–g).

2.10.3. Agarose gel electrophoresis

The DNA binding products were checked by agarose gel electrophoresis method (Abdel-Rahman et al., 2016b; 2017b,c,d,e,

Please cite this article in press as: Abdel-Rahman, L.H. et al., Design and nonlinear optical properties (NLO) using DFT approach of new Cr(III), VO(II), and Ni(II) chelates incorporating tri-dentate imine ligand for DNA interaction, antimicrobial, anticancer activities and molecular docking studies. Arabian Journal of Chemistry (2017), http://dx.doi.org/10.1016/j.arabjc.2017.07.007

f,g). Agarose (600 mg) was dissolved in hot tris-acetate-EDTA (TAE) buffer (60 mL) (4.84 g Tris base, pH-8.0, 0.5 M EDTA L–1) and heated to boil for few minutes. When the gel attains approximately 55 °C, it was then poured into the gas cassette fitted with comb. Slowly the gel was allowed to solidify by cooling to room temperature and then carefully the comb was removed. The solidified gel was placed in the electrophoresis chamber containing TAE buffer. The stock solution of complexes was prepared by solve 20 mg of the compounds in 20 ml of DMF. The sample (25 μg/ml) was added up to the separated DNA of Calf-thymus (CT-DNA) and incubated for 1 h at 37 ± 1 °C and then 30 μl of DNA sample (mixed with bromophenol blue dye at a 1:1 ratio) was charged on attention into the electrophoresis chamber wells along with a standard DNA marker in TBE buffer (50 mM Tris base, pH 7.2; 1 mM EDTA/1 L) and then loaded onto the agarose gel, then a constant electricity (60 V) was left for about 45 min. Finally, the gel was removed and spotted with 20 μg/ml of ethidium bromide for 10–20 min. The bands obtained was monitored under UV light using a transilluminator directed by photography with DMC-LZ5 Lumix Digital Camera to determine the extent of DNA binding as contrasted with standard DNA marker (Abdel-Rahman et al., 2013b; 2014a; 2015a,b; 2016a–c; 2017b–e).

2.11. Anticancer activity

The anticancer activity was made at the National Cancer Institute, Cancer Biology Department, Pharmacology Department, Cairo University. The absorbance or optical density (O.D.) of each well was estimated spectrophotometrically at 564 (nm) with an "ELIZA" micro plate reader (Meter tech. Σ 960, "USA"). Evaluation of the cytotoxic activity of the prepared ESAP imine ligand and its complexes was carried out against Colon carcinoma cells, (HCT-116 cell line), Breast carcinoma cells, (MCF-7 cell line) and hepatic cellular carcinoma cells (HepG-2 cell line). The evaluation process was carried out *in vitro* using the Sulfo-Rhodamine-B-stain (SRB) (Hindo et al., 2009; Abu-Dief et al., 2016; Abdel-Rahman et al., 2017c,d,e). Cells were placed in 96-multiwell plate (10^4 cells/well) for 24 h before processing with the complexes to allow attachment of cell to the wall of the plate. Various concentrations of the investigated compounds (0, 1, 2.5, 5 and 10 μM) were added to the cell monolayer. Monolayer cells were incubated with the complexes for 48 h at 37 °C and in atmosphere of 5% CO_2. After 48 hrs, cells were fixed, rinsed, and stained with Sulfo-Rhodamine-B-stain (Abu-Dief et al., 2016; Abdel-Rahman et al., 2017c,d,e). Excess stain was washed with acetic acid and attached stain was administered with Tris EDTA buffer. Color intensity was measured in an ELISA reader. IC_{50} was evaluated and potency was calculated with regard to percentage of change of (vistabline standard) (Abu-Dief et al., 2016; Abdel-Rahman et al., 2017c,d,e). The relation between surviving fraction and compound concentration is plotted to get the survival curve of each tumor cell line after the specified compound. The experiment was carried out once and each concentration repeated 3 times. The inhibitory concentration percent (IC %) was estimated (Abu-Dief et al., 2016; Abdel-Rahman et al., 2017c,d,e) according to the equation: Inhibition concentration

$$(\mathrm{IC})\ \% = (\text{Control O.D.} - \text{Ligand O.D.}) \times 100/\text{Control O.D} \quad (14)$$

2.12. Molecular docking study

Docking stimulation study is performed using molecular operating environment (MOE®) version 09.2014, Chemical Computing Group Inc., Montreal, Canada. The computational software operated under "Windows XP" installed on a Intel Pentium IV PC with a 1.6 GHz processor and 512 MB memory (Chemical Computing group, 2014).

Firstly, a Gaussian Contact surface around the binding site was sketched, then the surface enclosed the *van Waals* surface. Finally docking studies were done to assess the binding free energy of the inhibitor inside the macromolecule. The scoring in docking studies was done utilizing London dG scoring function. Each docking experiment was derived from 10 different runs were directed to analyze or achieving the best score. To compare the docking belonged to the ligand in the co-crystallized structure and to get RMSD of the docking pose database browser was used.

2.12.1. Preparation of ligands and target protein-tyrosine kinase

The compounds in this research as ligands were studied for their binding ability into protein-tyrosin kinase (TRK). The target compounds were constructed into a 3D model

Please cite this article in press as: Abdel-Rahman, L.H. et al., Design and nonlinear optical properties (NLO) using DFT approach of new Cr(III), VO(II), and Ni(II) chelates incorporating tri-dentate imine ligand for DNA interaction, antimicrobial, anticancer activities and molecular docking studies. Arabian Journal of Chemistry (2017), http://dx.doi.org/10.1016/j.arabjc.2017.07.007

using the builder interface of the MOE program after checking their structures and the formal changes on atoms by 2D depiction, the following steps were carried out: The target compounds were subjected to a conformational search. Conformers were subjected to energy minimization using MOE module until a RMSD gradient of 0.01 and RMS distance of 0.1 Å kcal mol^{-1} $Å^{-1}$ with MMFF94X force-field and the partial charges were automatically evaluated. The obtained database was then saved as MDB file to be used in the docking calculations. The X-ray crystallographic structure of c-kit receptor protein-tyrosine kinase in complex with STI-571 (Imatinib or Gleevec) were uploaded from the Protein Date Bank (PDB) (http://www.rcsb.org/pdb/explore/explore.do?structureId = 1T46) (PDB code: 1t46) was obtained from Protein data bank (Mol et al., 2004). Partial charges and hydrogen atom were set on to the protein with the protonation 3D application in MOE. This implementation is carried out to appropriate position hydrogen atom in the macromolecule structures and ionization states. Then four steps were made for both active sites: checking the atoms connection and type, adding hydrogen atoms to the system, selection of the receptor an fix it's atoms potential, MOE Alpha Site Finder was utilized for the active site search in the enzyme structure utilizing all default items. The active site was chosen to contain the residues that were bound to receptor. Dummy atoms were created from the obtained alpha Spheres.

2.12.2. Molecular modeling and analysis of the docked results

The binding affinity of the synthesized compounds to TRK protein by formation of the hydrogen bonds between the ligand and amino acid in TRK were carried out, which measured the hydrogen bond length, which does not surpass 3.7 Å. In addition, RMSD of the co-crystal ligand position compared to the docking pose was utilized in ranking. Both RMSD as well as the mode of interaction of the regional ligand within the crystal structure of c-kite tyrosin kinase receptor were carried out as the standard model.

3. Results and discussion

3.1. Physicochemical properties of the prepared ESAP imine ligand and its complexes

3.1.1. ^{1}H NMR and ^{13}C NMR spectra of the prepared ESAP imine ligand

The ^{1}H and ^{13}C NMR spectral data of the prepared ligand are recorded in the experimental section (cf Figs. S1 and S2). The ^{1}H NMR spectrum of ESAP imine ligand showed two singlet signals at δ = 13.90 and 9.61 ppm, that are assigned to the two phenolic —OH. The higher value of δ for the —OH group (13.90 ppm (s, 1H, 2′-OH) can be assigned to the presence of intermolecular hydrogen bonding (Abdel-Rahman et al., 2016c). Also, it shows singlet signal at δ = 8.94 which is characteristic for azomethine (CH═N) proton of the ligand (Abdel-Rahman et al., 2017c,d,e). Moreover, it shows multiplet signals at 7.18–6.99 ppm for aromatic of 9-CH protons. Furthermore, it shows one proton doublet at position 10. ^{13}C NMR of ESAP imine ligand exhibited signal at 162.15 ppm may be assigned to azomethine carbon. The signals observed in the region 152.70–15.28 ppm were assigned to phenyl carbons. The ^{1}H NMR spectra of the complexes cannot be obtained due to interference of their paramagnetic properties.

3.1.2. Elemental analysis and electrical conductivity measurements

All the prepared complexes are tinted, solid, steady at room temperature and non-hygroscopic in nature and possess high decomposition points (> 300 °C).

The elemental analysis results of the prepared imine ligand and its complexes are recorded in Table 1 and suggested that ESAP imine ligand act as tridentate and form complexes with VO(II), Cr(III) and Ni(II) in 1:1 ratio metal to ligand (cf. Scheme 1). The molar conductance of all the prepared complexes was observed at room temperature in DMF as a solvent and their results in (Ω^{-1} cm^2 mol^{-1}) are recorded in Table 1. The molar conductance values of ESAPNi and ESAPV complexes at room temperature are 2.55 and 10.35 Ω^{-1} cm^2 mol^{-1}, respectively assigned to their non-electrolytic nature whereas ESAP with 68 Ω^{-1} cm^2 mol^{-1} is electrolyte species (Abdel-Rahman et al., 2013a,b; 2014a;2015a,b; 2016a,b,c; 2017b,c,d,e).

3.1.3. Infrared spectra

In order to study the bonding mode of ligand to metal in the complexes, IR spectrum of the free ligand was compared with the spectra of metal complexes. The fundamental infrared spectral frequencies of the ESAP ligand its complexes along with their assignments are shown in (Table 2). Bands due to —OH and —CH═N are distinguishable and offer proof regarding the structure of the ligand and its bonding with metal (cf. Figs. S3 and S4). A band at 1627 cm^{-1} in the ESAP ligand is due to —C═N stretching vibration. On complexation, this band is dislodged to a lower frequency (1602–1620 cm^{-1}). The negative shift of this band is an obvious indication of the participation of the azomethine nitrogen atoms in complex formation (Abdel-Rahman et al., 2013a,b; 2014a; 2015a,b; 2017b,c,d,e). This is supported by the appearance of band at 430–499 cm^{-1} corresponding to the stretching vibration of M—N bond. Bands at 537–597 cm^{-1} correspond to M—O stretching vibrations. Band at 3424 cm^{-1} observed in the ligand spectrum is due to stretching vibrations of free —OH. In the complexes, the recorded IR spectra of all the prepared imine complexes show broad band at 3380–3418 cm^{-1} which have been assigned to υ(OH) stretching vibration of hydrated water molecules, in correspondence with the findings of the elemental analysis listed in (Table 2). A band at 968–976 cm^{-1} (OH rocking) suggests the presence of coordinated water in all three complexes. In the low frequency zone, the band observed for ESAP imine ligand showed an absorption band at 1227 cm^{-1} which can result from the stretching vibration of the phenolic (C—O) group. The displace of that band to lower wave number values upon complexation indicates that the oxygen atoms of the phenolic groups are coordinated to the metal ion. The characteristic frequencies of the coordinating nitrate group in ESAPCr complex possess three non-degenerated modes at 1470 cm^{-1} υ(NO_2)asy, 1356 cm^{-1} υ(NO_2)sy and 858 cm^{-1} υ(NO) (Abdel-Rahman et al., 2017d)

Please cite this article in press as: Abdel-Rahman, L.H. et al., Design and nonlinear optical properties (NLO) using DFT approach of new Cr(III), VO(II), and Ni(II) chelates incorporating tri-dentate imine ligand for DNA interaction, antimicrobial, anticancer activities and molecular docking studies. Arabian Journal of Chemistry (2017), http://dx.doi.org/10.1016/j.arabjc.2017.07.007

Table 1 Analytical and physical data of the titled ESAP imine ligand and its complexes.

Compounds (Molecular formula)	M.wt	Color Yield (%)	Λ_m (Ω^{-1} cm^2 mol^{-1})	μ_{eff} (B.M.)	M.p and Dec. temp (°C)	Analysis (%) Found (calcd.)		
						C	H	N
ESAP $C_{15}H_{15}NO_3$	257.11	Orange (92)	–	–	190	70.18 (70.02)	5.75 (5.88)	5.47 (5.44)
ESAPNi $C_{17}H_{19}NiNO_4$	359.69	Green (90)	2.55	2.62	(> 300)	56.49 (56.71)	5.31 (5.28)	3.84 (3.89)
ESAPV $C_{15}H_{15}NO_5V$	340.04	Deep green (86)	10.35	1.71	(> 300)	52.77 (52.93)	4.49 (4.44)	4.03 (4.12)
ESAPCr $C_{15}H_{19}N_2O_9Cr$	423	Black (91)	68	3.76	(> 300)	42.51 (42.55)	4.47 (4.49)	6.59 (6.62)

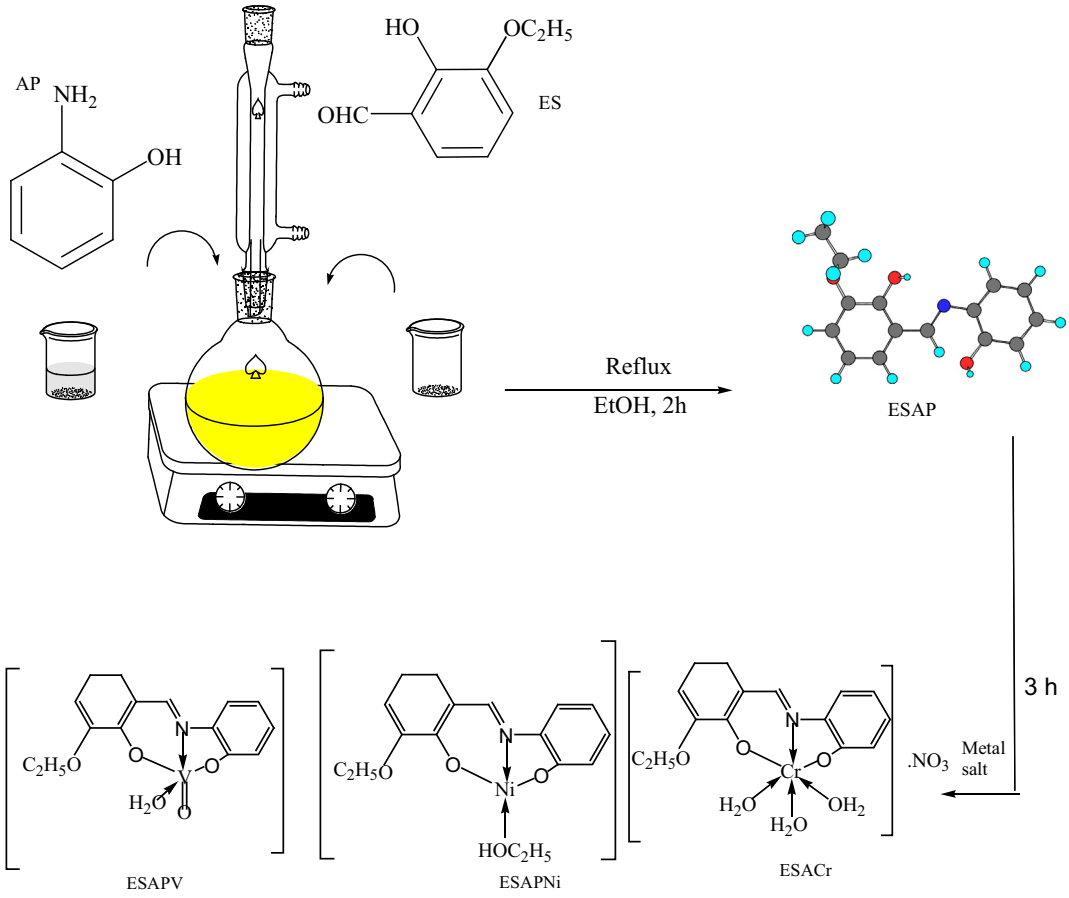

Scheme 1 Synthetic strategy for the preparation of the investigated complexes.

3.1.4. Electronic spectra

The molecular electronic absorption spectra are often very important in the evaluation of results furnished by other methods of check. The numerical values of the maximum absorption wavelength (ε_{max}) and the molar absorptivity (λ_{max}) were listed in TableS1 and the spectra were presented in Fig. 1. The electronic spectral measurements were utilized for assigning the stereo chemistries of metal ions in the complexes relying on the sites and number of *d–d* transition peaks (Chen et al., 2009). The electronic absorption spectra of ligands and their complexes were registered at the wavelength range 800–200 nm and 298 K. The ligand exhibits absorption bands in UV–Vis region around 400 nm which is assigned to $n \rightarrow \pi^*$ transition originating from the imine function of the imine ligand (Silverstein and Webster., 1997). The absorption bands of complexes at λ_{max} = 306–471 nm is assigned to charge transfer with in ESAP imine ligand to the metal ion. These charge-transfer transitions probably occur form the p-orbitals of the Schiff bases to the d-orbitals of metal ion. Another difference observed in the electronic spectra of the prepared complexes, compared to the spectra of the corresponding free ligand, is associated with the appearance of a broad low intensity band. This a long and a broad band lying in the region 504–524 nm (ε_{max} = 230–570 mol^{-1} cm^2). This band could be mainly attributed to the $d \rightarrow d$ transition in the structure of the prepared complexes (cf. Table S1) (Dyer, 1965). These bands are of low molar absorptivity, Ɛ, being Laporte 'forbidden' transitions.

Please cite this article in press as: Abdel-Rahman, L.H. et al., Design and nonlinear optical properties (NLO) using DFT approach of new Cr(III), VO(II), and Ni(II) chelates incorporating tri-dentate imine ligand for DNA interaction, antimicrobial, anticancer activities and molecular docking studies. Arabian Journal of Chemistry (2017), http://dx.doi.org/10.1016/j.arabjc.2017.07.007

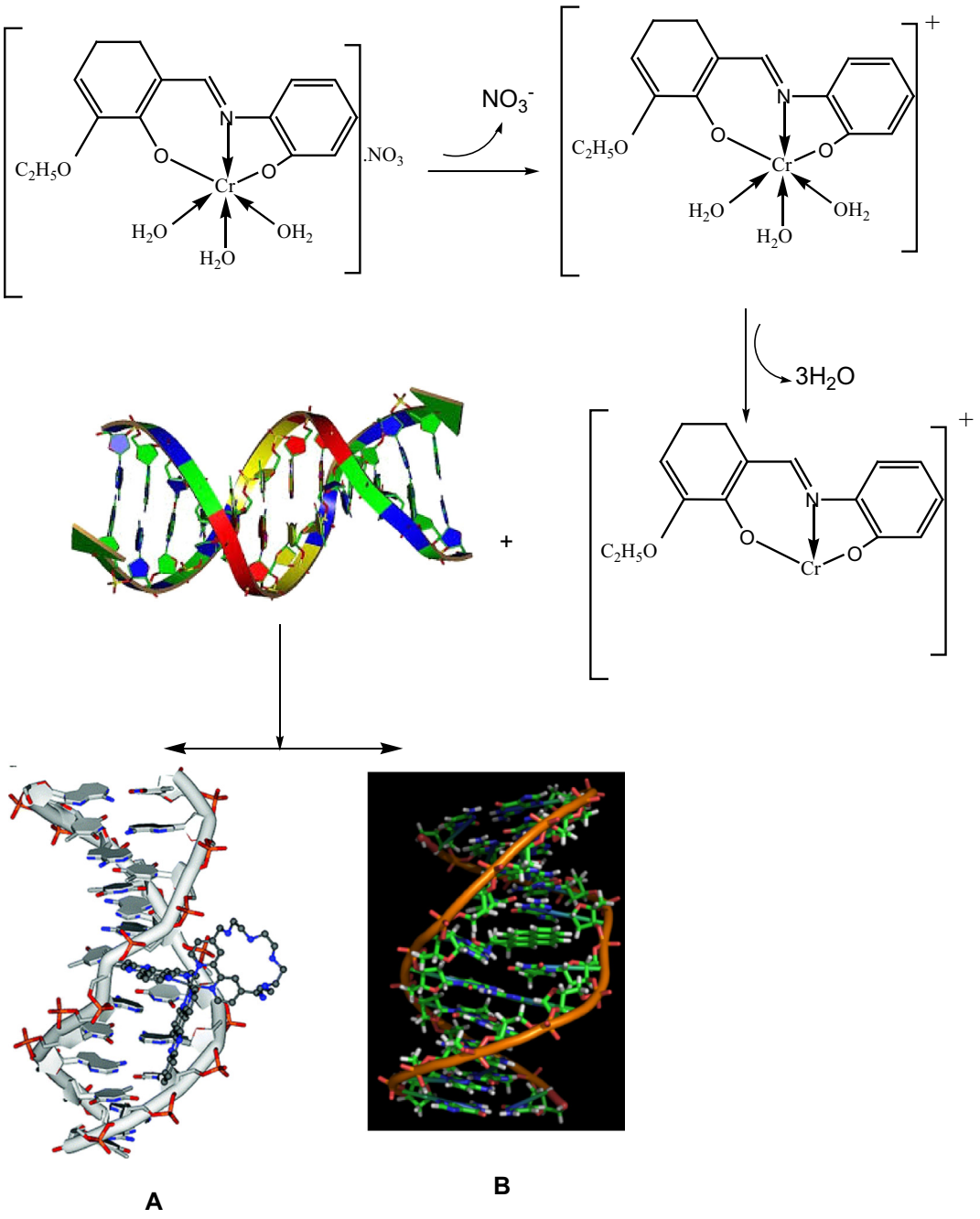

Scheme 2a Suggested mechanism for interaction of ESAPCr with DNA via (A) intercalation binding and (B) replacement.

3.1.5. Magnetic susceptibility measurements

The magnetic susceptibility measurements give information considering the geometric structure of the compounds. The observed magnetic moment for complexes are generally diagnostic of the coordination geometry about the metal ion (cf. Table 1). ESAPCr complexes show magnetic moments corresponding to three unpaired electrons, i.e. (3.76 B.M.), as expected for octahedral Cr(III) complexes (Alaghaz et al., 2015). The magnetic moment values of Ni(II) complexes is 2.62 BM, indicating the presence of two unpaired electrons per Ni(II) ion and suggesting these complexes to have tetrahedral geometry (Ismail et al., 2012). The magnetic susceptibility of ESAPV complex has a magnetic moment value of 1.71 B. M., which is close to the spin-only value for d^1 and in agreement with the reported values for distorted octahedral complexes of VO(II) (Sarkar et al., 2007).

3.1.6. Thermal analysis

Thermal analysis (TGA) of the metal chelates is an important tool for (i) get information about the thermal stability of these complexes, (ii) decide whether the water molecules (if present) are inside or outside the inner coordination sphere of the central metal ion.

The thermal stabilities were investigated for imine complexes have been studied as a function of temperature. The proposed stepwise thermal degradation of the complexes with

Please cite this article in press as: Abdel-Rahman, L.H. et al., Design and nonlinear optical properties (NLO) using DFT approach of new Cr(III), VO(II), and Ni(II) chelates incorporating tri-dentate imine ligand for DNA interaction, antimicrobial, anticancer activities and molecular docking studies. Arabian Journal of Chemistry (2017), http://dx.doi.org/10.1016/j.arabjc.2017.07.007

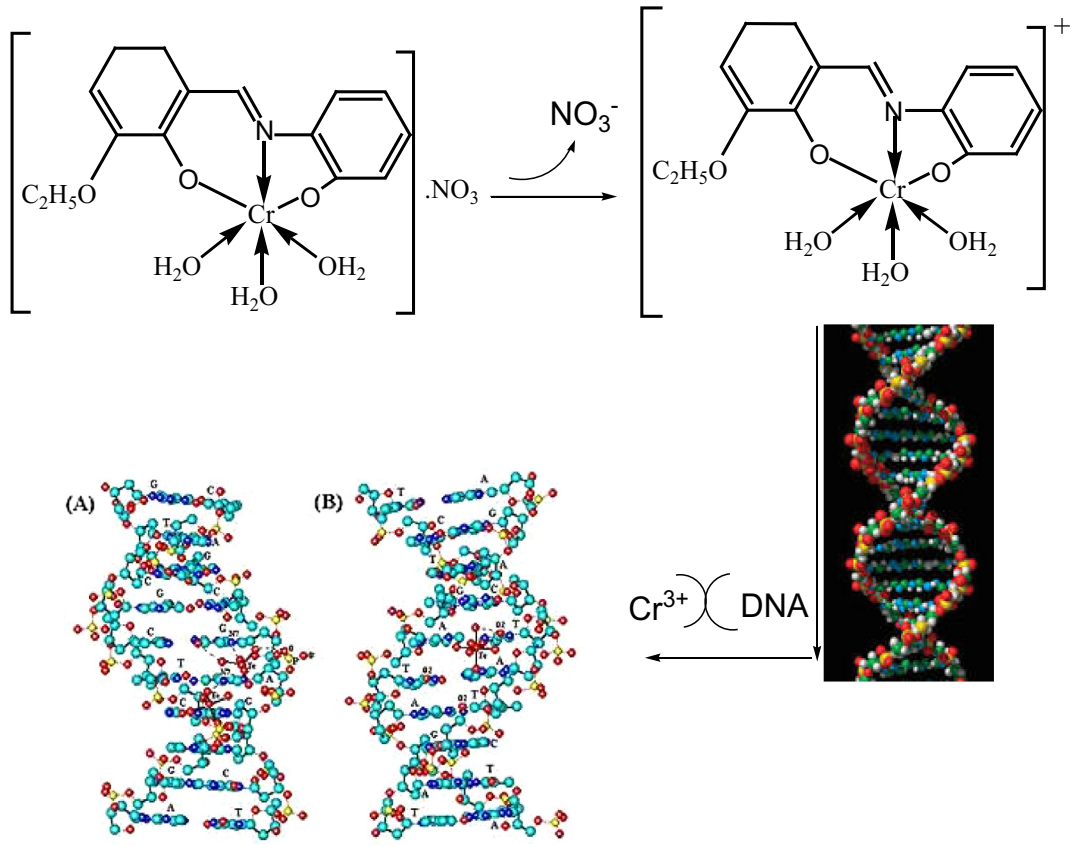

Scheme 2b Suggested mechanism for interaction of ESAPCr with DNA via groove binding (electrostatic and hydrogen bond).

Table 2 Characteristic IR bands of the prepared ESAP imine ligand and its complexes.

Compounds	$\upsilon(OH)/H_2O$	$\upsilon(CH)_{ar}$	$\upsilon(C{=}N)$ vs	$\upsilon(C{-}O)_{ph}$	$\upsilon\ (M{-}N)_w$	$\upsilon(M{-}O)_m$
ESAP	3426(s)	3061	1627	1227	–	–
ESAPV	3524	3058	1603	1225	597	542
ESAPNi	3380	3058	1620	1224	563	499
ESAPCr	3392	3065	1602	1215	752	537

vs = very strong, s = strong, m = medium, w = weak, ar = aromatic, ph = phenolic.

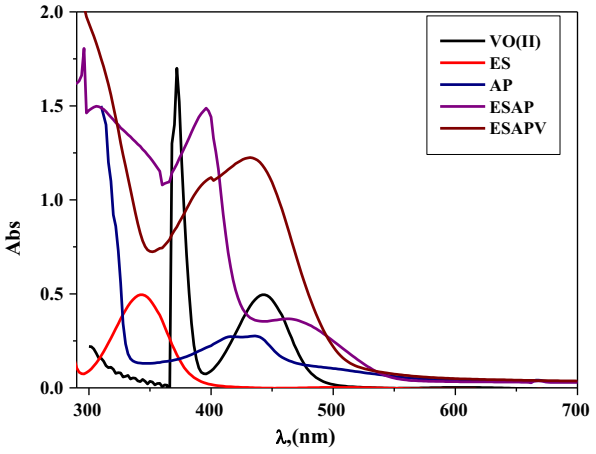

Fig. 1 Molecular electronic spectra of 10^{-3} M of ESAPV complex and its components in DMF at 298 K.

respect to temperature and the formation of respective metal are depicted in Table 3. The thermograms of the prepared imine complexes confirm the presence one molecule of coordinated water in case of ESAPV complex and three coordinated water molecules in case ESAPCr complex (cf. Scheme 1). The thermal behavior of the metal complexes showed that the hydrated complexes lose water molecules of hydration in the first step; then lose coordinated water molecules with decomposition of the ligand molecules in the subsequent steps as shown in (Table 3).

The thermogram of **ESAPV** complex showed three stages of decomposition up to 604 °C. It dehydrates one water molecule in the first step up to 122 °C. During furthers heating, the **ESAPV** complex complete decomposition in two steps and shows mass losses of about 35.10% (Calc. 35.00%), 39. 92% (Calc. 40.01%) in the temperature ranges of 124–430 °C, 432–604 °C, respectively leaving VO(II) as a residue.

The TGA curve of ESAPCr complex show loss in weight within the temperature range 35–301 °C, which is due to

Please cite this article in press as: Abdel-Rahman, L.H. et al., Design and nonlinear optical properties (NLO) using DFT approach of new Cr(III), VO(II), and Ni(II) chelates incorporating tri-dentate imine ligand for DNA interaction, antimicrobial, anticancer activities and molecular docking studies. Arabian Journal of Chemistry (2017), http://dx.doi.org/10.1016/j.arabjc.2017.07.007

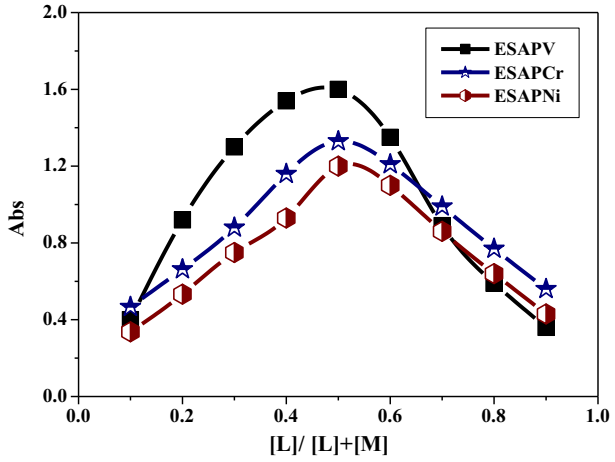

Fig. 2 Continuous variation plots for the prepared complexes in aqueous – ethanolic medium at (ESAPV) = (ESAPCr) = (ESAPNi) = 10^{-3} M and 298 K.

removal of the lattice nitrate and three coordinated water molecules (Found 27.48%, Calc. 27.43%). Also, the ESAPCr complex shows mass loss within the temperature range 303–486 °C, which is due to removal of the part of ligand ($C_8H_8O_2$) with mass losses (Found 32.18%, Calc. 32.15%). Finally the complexes undergo decomposition of the organic ligand within the temperature range up to 635 °C with mass losses (Found 28.09%, Calc. 28.13%), leading to the formation of Cr as final product (Shakir et al., 2016; Abdel-Rahman et al., 2017b).

The thermogram of the **ESAPNi** complex showed three decomposition steps within temperature range 33–486 °C. The first step of decomposition within the temperature range from 33 to 149 °C correspond to the loss of coordinated ethanol molecule, with a mass loss of 12.69% (Calc. 12.79%). The second step of decomposition within the temperature range 151–301 °C with mass loss of 37.83% (Calc. 37.80%) indicated that removal of part of imine ligand ($C_8H_8O_2$). The third stage in the temperature range 303–486 °C, an estimated mass loss of 33.12% (calc. 33.08%). This mass correspond to loss of the remaining part of ligand (C_7H_5NO) leaving Ni as a residue (Shakir et al., 2016; Abdel-Rahman et al., 2016c; 2017b). The horizontal lines in the TGA curves beyond 650 °C have been observed in all the metal complexes indicated no further weight loss, implying that a metal residue may be the final product. The thermal analysis data agree well with the proposed stoichiometry derived from the results of elemental analysis findings.

3.1.6.1. Kinetic aspects. The Kinetic parameters are shown in Table 3. It is shown that G^* values increase due to increasing temperature. The positive values of H^* show that degradation processes are endothermic. In most thermal steps, S^* values are negative suggesting a decomposition via abnormal pathway at those steps and the degeneration processes are undesirable. The negative activation entropy values give evidence for a more ordered activated state. This can be valid through the chemisorption of oxygen and other decomposition products. The nature of the more ordered can be assigned to the bonds polarization of the activated state which taken place through electronic transitions. Finally, positive values were found for H^* and G^* respectively, performing endothermic character for all thermal steps (Abdel-Rahman et al., 2016a,b,c; 2017a,b).

3.1.7. Spectrophotometric determination of the stoichiometry of the prepared complexes

Stoichiometry of the prepared complexes is defined utilizing the two methods involving the use of spectrophotometry, namely, continuous-variations method and mole-ratio method. Based on the methods which were utilized and the experimental results, the stoichiometry of the prepared complexes is 1:1. The curves of the continuous variation method (cf. Fig. 2) displayed maximum absorbance at mole fraction X_{ligand} = 0.5–0.6 showing the complexation of metal ions to ligand in molar ratio 1:1. Moreover, the data resulted from utilizing the molar ratio method support the same metal ion to ligand ratio of the prepared complexes (cf. Fig. S5)

Table 3 Thermal decomposition steps, mass loss (%), proposed lost segments, final residue thermo-kinetic activation parameters of each decomposition step for the prepared complexes.

Complex	Decomp. Temp. (°C)	Mass loss (%)		proposed segment	E^* (kJ mol^{-1})	A (S^{-1})	ΔH^* (kJ mol^{-1})	ΔG^* (kJ mol^{-1})	ΔS^* (J mol^{-1} K^{-1})
		Found	(Calc.)						
ESAPV	34–122	5.31	(5.29)	H_2O	51.8	0.12	51	68.3	−250.4
	124–430	35.10	(35.00)	C_7H_5NO			49.5	122	−261.97
	432–604	39.92	(40.01)	$C_8H_8O_2$			47.5	187.3	−267.3
Residue	> 604	19.66	(19.69)	VO			–	–	–
ESAPCr	35–301	$3H_2O$ + NO_3	116	27.48	314	0.25	313	357	−252
	303–486	$C_8H_8O_2$	136	32.18			311	410	−258.8
	488–635	C_7H_5NO	119	28.09			309	456	−261.75
Residue	> 635	Cr	52	12.32			–	–	–
ESAPNi	33–149	12.69	(12.79)	C_2H_5OH	98	0.26	97.3	118.7	−245.9
	149–301	37.83	(37.80)	$C_8H_8O_2$			96.2	152.3	−253.7
	301–486	33.12	(33.08)	C_7H_5NO			94.7	196.8	−258.5
Residue	> 486	16.44	(16.32)	Ni			–	–	–

Please cite this article in press as: Abdel-Rahman, L.H. et al., Design and nonlinear optical properties (NLO) using DFT approach of new Cr(III), VO(II), and Ni(II) chelates incorporating tri-dentate imine ligand for DNA interaction, antimicrobial, anticancer activities and molecular docking studies. Arabian Journal of Chemistry (2017), http://dx.doi.org/10.1016/j.arabjc.2017.07.007

Table 4 The formation constant (K_f), stability constant (pK) and Gibbs free energy $\Delta(G^*)$ values of the synthesized complexes at 298 K.

Complex	Type of complex	K_f	Log K_f	ΔG^* (kJ mol^{-1})
ESAPNi	1:1	4.09×10^4	4.61	−26.31
ESAPCr	1:1	2.56×10^4	4.41	−25.15
ESAPV	1:1	1.26×10^4	4.10	−23.39

(Abdel-Rahman et al., 2013a,b; 2014a; 2015a,b; 2016a,b,c,d; 2017a,b,d,e).

3.1.7.1. Determination of the apparent formation constants of the synthesized complexes. The formation constants (K_f) of the studied imine complexes formed in solution were obtained from the spectrophotometric measures by utilizing the continuous variation method (cf. Table 4). The obtained K_f values show the high stability of the tested complexes. The values of K_f for the checked complexes increase in the following order: ESAPNi > ESAPCr > ESAPV complex. Moreover, the values of the stability constant (pK) and Gibbs free energy ($\Delta G^{\neq}$) of the presented complexes are calculated. The negative values of Gibbs free energy mean that the reaction is spontaneous and preferable. The pH-profile (absorbance vs. pH) explained in (cf. Fig. 3) showed typical dissociation curves and a high stability pH extent (4–9) of the checked complexes. This indicates that the formation of the complex greatly stabilizes imine ligands. Consequently, the suitable pH range for the different applications of the tested complexes is from pH = 4 to pH = 9 rely on the finding of elemental analyses, molar conductance, magnetic measures, infrared and electronic spectra, the suggested composition of the complexes was identified.

3.1.8. Molecular orbital calculations

The optimized geometrical parameters (bond lengths, bond angles and dihedral angles), natural charges (valence, core, Rydberg and total) on active centers, natural configuration of the metal ions, natural population and energetic of the ground state for the studied complexes are calculated and discussed using B3LYP/GEN and B3LYP/LANL2DZ. From the elemental analysis and spectroscopic data, metal ions coordinated to the ligand via N8, O15 and O16 atoms, two water molecules and OH^- ion in case of Cr forming octahedral complex . In case of ESAPNi complex, the metal ion coordinated to the ligand via N8, O16 and O15-atoms and ethyl alcohol molecule forming tetrahedral complex. In ESAPV complex, the central metal ion coordinated to N8, O15 and O16-atoms and one water forming square pyramidal structure.

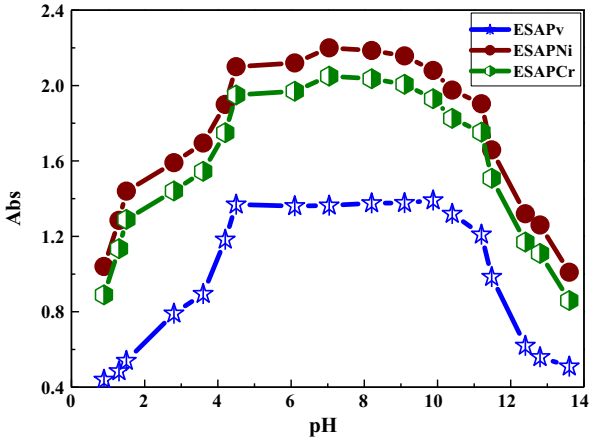

Fig. 3 Dissociation curve of the prepared imine complexes in DMF.

3.1.8.1. Structure of the prepared complexes. The optimized geometry, numbering system, vector of the dipole moment, bond lengths, bond angles and dihedral angles of all metal complexes studied in this work are presented in Table 5 and Fig. 4. In ESAPCr complex, the metal ion coordinates with O15, N8 and O16 atoms forming five membered rings namely, MO15C14C9N8, six membered rings, namely, MO16C5C6C7N8, two water molecules and OH^- ion to form octahedral structure. In case of ESAPNi complex, the metal ion coordinates with O15, N8 and O16 to form five membered rings namely, MO15C14C9N8, six membered rings, namely, MO16C5C6C7N8 and with one ethyl alcohol molecule to form tetrahedral structure. In case of ESAPV complex, the metal ion coordinates with O15, N8 and O16 to form five membered ring namely, MO15C14C9N8, six membered ring, namely, MO16C5C6C7N8 and water molecule to form square pyramidal structure. Therefore, distortions from regular octahedral, tetrahedral and square pyramidal geometry are expected for all the studied complexes. In the studied complexes, most of

Table 5 Optimized bond lengths, bond angles and dihedral angles of the studied complexes using B3LYP/GEN.

Parameter	ESAPV	ESAPCr	ESAPNi
M—O16, Å	1.671	1.746	1.625
M—N8	1.984	1.644	1.741
M—O15	1.912	1.659	1.688
M—O21	2.037	1.972	1.779
M—O22		2.145	
M—O23		2.338	
<O16MO23		87.6	
<O16MN8	87.8	86.2	93.1
<N8MO15	43.4	51.3	44.4
<O15MO22		57.6	
<O22MO21		49.7	
<O15MO21	90.6		
<O21MO16	86.3		
<N8MO15	83.7		
<N8MO16	87.8		
<O21MO23		57.3	
<O23MN8C9		−74.7	
<O22MO15C14		110.2	
<O21MO15C14	−170.6	26.9	−154.7
<O21MO16C5	138.7	−92.4	111.8

Please cite this article in press as: Abdel-Rahman, L.H. et al., Design and nonlinear optical properties (NLO) using DFT approach of new Cr(III), VO(II), and Ni(II) chelates incorporating tri-dentate imine ligand for DNA interaction, antimicrobial, anticancer activities and molecular docking studies. Arabian Journal of Chemistry (2017), http://dx.doi.org/10.1016/j.arabjc.2017.07.007

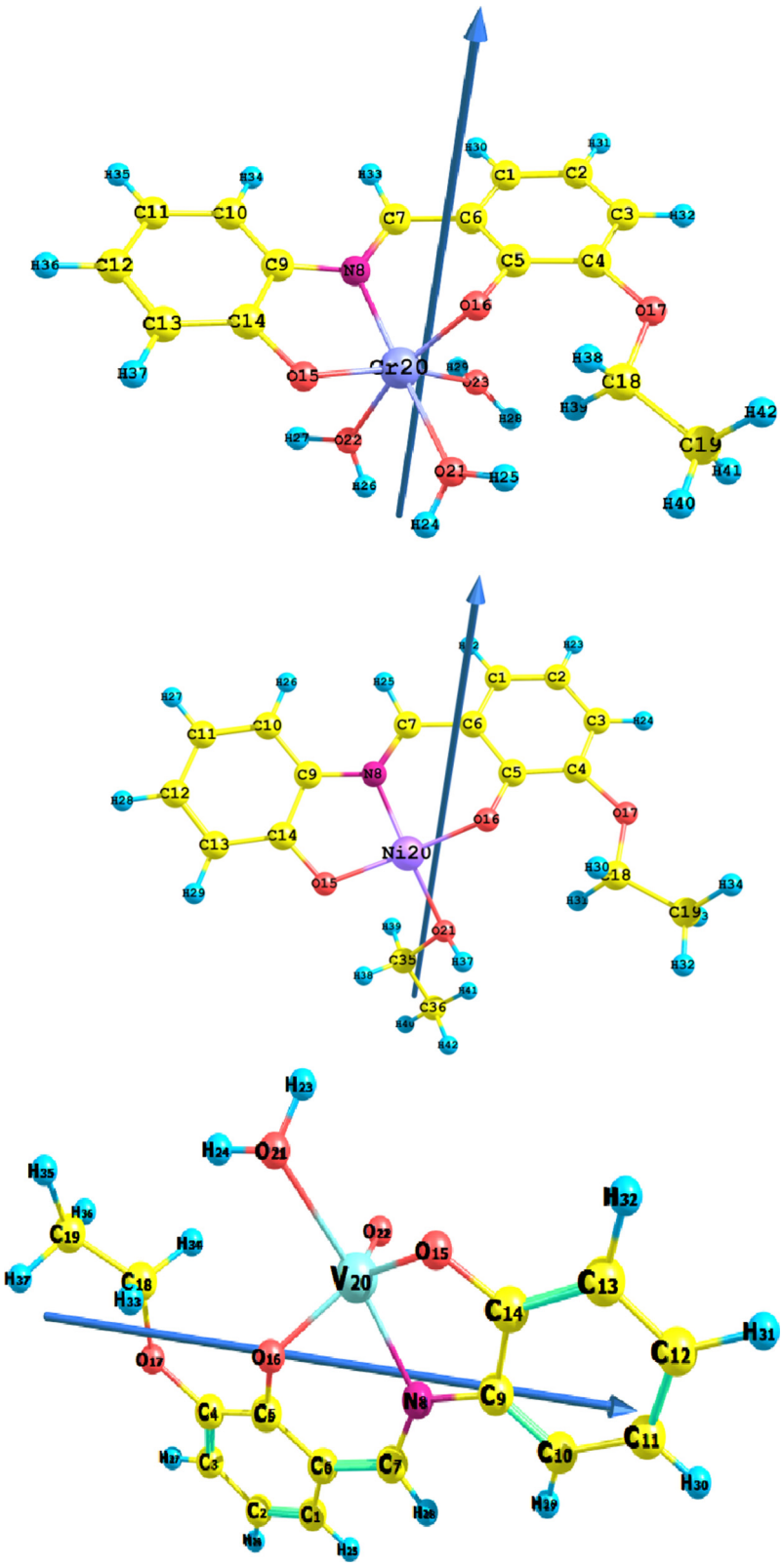

Fig. 4 The optimized geometry, the vector of the dipole moment and numbering system for the studied complexes using B3LYP/GEN.

M—N and M—O bonds show elongation upon complexation. The elongation of the M—N bond length is greater than M—O bonds in the studied complexes. The length of the coordinate covalent bonds between metal and ligand site, i.e. M—N, and M—O, are too long compared to the typical MX bond lengths (Abdel-Rahman et al., 2016d). The too long M—O

Please cite this article in press as: Abdel-Rahman, L.H. et al., Design and nonlinear optical properties (NLO) using DFT approach of new Cr(III), VO(II), and Ni(II) chelates incorporating tri-dentate imine ligand for DNA interaction, antimicrobial, anticancer activities and molecular docking studies. Arabian Journal of Chemistry (2017), http://dx.doi.org/10.1016/j.arabjc.2017.07.007

Table 6 Total energy, E_T, energy of HOMO and LUMO, energy gap, Eg, ionization energy, I, electron affinity, A, electronegativity, X, Hardness, η, softness, s and chemical potential, v, of the studied complexes using B3LYP/LANL2DZ.

Parameter	ESAPV	ESAPCr	ESAPNi
E_{HOMO}, a.u.	−0.2119	−0.3165	−0.1923
E_{LUMO}, a.u.	−0.0950	−0.2110	−0.0766
E_g, eV	3.179	2.869	3.147
I, eV	5.763	8.608	5.231
A, eV	2.584	5.739	2.084
X, eV	4.174	7.174	3.657
η, eV	1.589	1.435	1.574
S, eV^{-1}	0.315	0.348	0.318
v, eV	−4.174	−7.174	−3.65

and M—N bonds in the complexes mean that the ionic character of these bonds is small. The bond angles between metal ion and binding sites in the coordination sphere (c.f. Tables 5) in the ESAPCr complex vary between 49° and 86° which compare nicely with the experimental data as obtained from X-ray analysis for O_h complexes (Armelao et al., 2010) which indicate a distorted octahedral geometry. Also a distortion from tetrahedral of ESAPNi complex and square pyramidal of ESAPV complex is observed from bond angles of the coordination spheres (c.f. Table 5). The values of the dihedral angles around metal ion in the coordination sphere in the studied complexes (c.f. Tables 5) are far from 0° or 180° which indicate that the metal ion is not in the same plane as the donating sites.

3.1.8.2. Natural charges and natural population. The natural charges on the coordinated atoms and the accumulation of electrons in the core, valence and rydberg sub-shells and natural electronic configuration of the metal ions in the coordination sphere of the studied complexes are presented in Tables S2 and S3. The most electronegative charges are accumulated on N8, O15, and O16. These electronegative atoms have a tendency to donate electrons. Whereas, the most electropositive atoms such as; V, Cr and Ni have a tendency to accept electrons. In V-complex, the central metal ion received 3.1232e

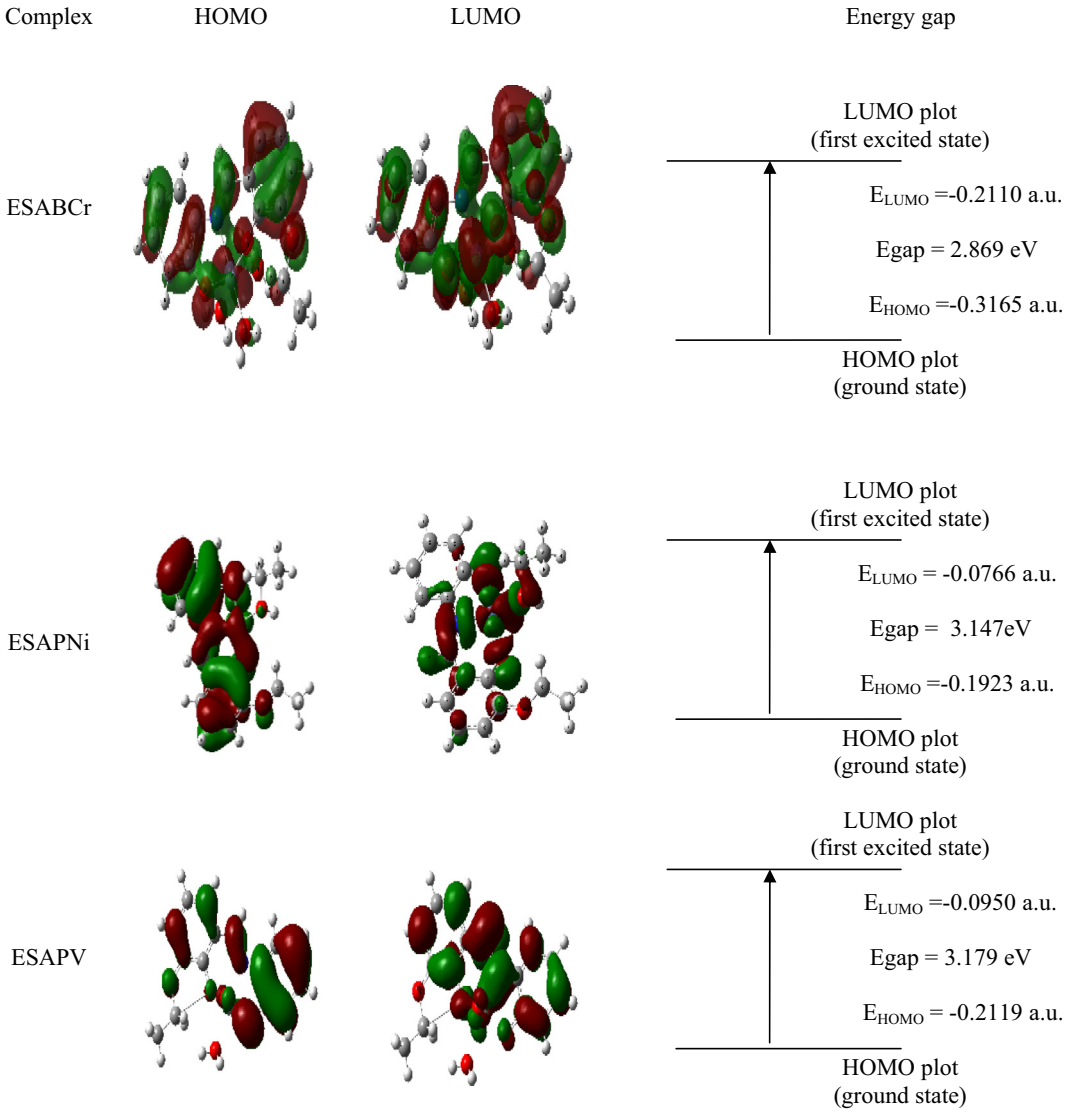

Fig. 5 HOMO-LUMO charge density maps and energy gap of the studied complexes using B3LYP/LANL2DZ.

Table 7 Total static dipole moment, μ, the mean polarizing, α, the anisotropy of the polarizibility, Δα and the first-order hyperpolarizibility, β, for the ligand and the studied complexes using B3LYP/LANL2DZ.

Property	Urea	ESAP	ESAPV	ESAPCr	ESAPNi
μ_x		−3.1933	−1.1128	0.6368	−0.3159
μ_y		1.6374	−0.3188	−4.9186	2.8428
μ_z		0.5403	−0.2237	8.2028	2.0849
μ_D	1.3197	3.6291	1.1789	9.5854	3.5396
α_{xx}, a.u.		−105.2	−126.07	−103.01	−145.30
α_{xy}		−8.36	12.38	8.51	7.58
α_{yy}		−96.9	−104.21	−90.13	−112.62
α_{zz}		−122.5	−150.66	−122.47	−144.47
α_{yz}		−1.78	−0.048	−9.92	−1.32
α_{xz}		1.93	−1.271	−2.29	−2.99
α, a.u., esu		−108.2	−126.98	−105.20	−134.13
		1.603×10^{-23}	1.8818×10^{-23}	1.5591×10^{-23}	1.9878×10^{-23}
α, a.u. Δ, esu		22.6	40.25	28.1998	32.27
		3.349×10^{-24}	5.9651×10^{-24}	4.1732×10^{-24}	4.7824×10^{-24}
β_{xxx}, a.u.		−20.3	42.58	102.91	−45.0
β_{xxy}		−1.7	−20.0	−12.59	15.53
β_{xyy}		−34.8	−35.92	−30.71	2.93
β_{yyy}		51.2	−78.62	−98.29	90.57
β_{xxz}		−8.1	2.55	−5.15	−6.72
β_{xyz}		−0.64	−3.40	−20.91	−14.80
β_{yyz}		−1.4	24.99	53.58	28.23
β_{xzz}		5.1	−18.66	−11.07	16.44
β_{yzz}		14.1	−18.57	−68.43	36.25
β_{zzz}		1.62	−8.37	91.75	−8.42
β, a.u., esu		81.28	14244.99	55539.39	21091.765
	0.1947×10^{-30}	7.022×10^{-31}	1.2306×10^{-28}	4.7982×10^{-28}	1.8222×10^{-28}

($3d^{3.56}$), in Cr-complex, the metal ion received 2.1277e ($3d^{4.57}$) and in ESAPNi complex, Ni-ion received 1.2243e ($3d^{8.76}$) from the active sites of the ligands. Total Lewis (effective core, core and valence Lewis) and total non-Lewis (valence non-Lewis and rydberg non-Lewis) of the studied complexes are presented in Table S3.

3.1.8.3. Global reactivity descriptors. They include HOMO, LUMO, energy gap (E_g), chemical hardness (η), electronegativity (X), chemical potential (V), electron affinity (A), ionization potential (I) and global softness (S). The frontier molecular orbital (FMO) energies of the studied complexes were calculated using B3LYP/LANL2DZ and presented in Table 6 and Fig. 5. Energy gap (E_g) between HOMO and LUMO characterizes the molecular chemical stability (reactivity). The results in Fig. 5 and Table 6 indicate that the smaller the energy gap the easier the charge transfer and the polarization occurs within the molecule. The order of increasing reactivity in the studied complexes is: ESAPCr > ESAPNi > ESAPV. Using HOMO and LUMO energies, ionization potential and electron affinity can be expressed as $I \sim -E_{HOMO}$, $A \sim -E_{LUMO}$, the chemical hardness (η) = (I − A)/2, electronegativity (X) = (I + A)/2, chemical potential (V) = −(I + A)/2 and chemical global softness (S) = 1/2η values are calculated and presented in Table 6. The variation of electronegativity (X) values is supported by electrostatic potential, the results in Table 6 shows that the orders of decreasing X (increasing CT within the complexes) are: ESAPCr > ESAPV > ESAPNi. The small η values for the studied complexes reflect the ability of charge transfer inside the complexes. Therefore, the order of increasing the charge transfer within the studied complexes is: ESAPCr > ESAPNi > ESAPV which is the same order of reactivity.

3.1.8.4. Non-linear optical properties (NLO). So far no experimental or theoretical investigations were found addressing NLO for these classes of complexes; therefore, this triggered our interest to undertake this study.

NLO is at the forefront of current research because of its importance in providing key functions of frequency shifting, optical modulation, switching, laser, fiber, optical materials logic and optical memory for the emerging technologies in region such as telecommunications, signal processing and optical inter connections (Zumdahl et al., 2000). In order to investigate the relationship between molecular structure and NLO, the polarizibilities and hyperpolarizibilities of the studied complexes are calculated using B3LYP/LANL2DZ (Natorajan et al., 2008; Chemia and Zysss, 1987; Bradshow and Andrews, 2009). Total static dipole moment (μ), the mean polarizibility (α) the anisotropy of the polarizability (Δα) and the mean first-order hyperpolarizibility (β) of the ligand and the studied complexes are listed in Table 7 The polarizibilities and first-order hyperpolarizibilities are recorded in atomic units (a.u.), the calculated values have been converted into electrostatic units (esu) using conversion factor of 0.1482×10^{-24} esu for α and 8.6393×10^{-33} esu for β. Urea is a standard prototype used in NLO studies. In this study, Urea is chosen as a reference as there were no experimental values of NLO properties of the studied complexes. The magnitude of the molecular hyperpolarizibility β is one of the key factors in NLO system. The analysis of the β parameter show that the ligand ESAP is ~4 times higher than urea. The value

Please cite this article in press as: Abdel-Rahman, L.H. et al., Design and nonlinear optical properties (NLO) using DFT approach of new Cr(III), VO(II), and Ni(II) chelates incorporating tri-dentate imine ligand for DNA interaction, antimicrobial, anticancer activities and molecular docking studies. Arabian Journal of Chemistry (2017), http://dx.doi.org/10.1016/j.arabjc.2017.07.007

Table 8 Results of activity index of the prepared Schiff base ligand and its complexes against different strains of bacteria and fungi.

Compounds	±SD Inhibition zone (mm)											
	Escherichia coli (−ve)		*Bacillus subtilis* (+)		*Staphylococcus aureus* (+ve)		*Candida albicans*		*Aspergillus flavus*		*Trichophyton rubrum*	
Conc. (mg/ml)	10	20	10	20	10	20	10	20	10	20	10	20
ESAP	6 ± 0.11	12 ± 0.59	7 ± 0.37	16 ± 0.73	7 ± 0.09	14 ± 0.89	6 ± 0.14	9 ± 0.18	4 ± 0.69	7 ± 0.89	4 ± 0.33	6 ± 0.23
ESAPV	16 ± 0.63	34 ± 0.10	21 ± 0.86	46 ± 0.20	18 ± 0.48	37 ± 0.55	18 ± 0.42	28 ± 0.47	12 ± 0.39	25 ± 0.27	10 ± 0.47	20 ± 0.68
ESAPNi	15 ± 0.88	33 ± 0.87	20 ± 0.77	44 ± 0.07	17 ± 0.87	36 ± 0.13	18 ± 0.68	28 ± 0.02	11 ± 0.44	24 ± 0.63	10 ± 0.78	19 ± 0.30
ESAPCr	17 ± 0.59	33 ± 0.01	20 ± 0.76	45 ± 0.85	19 ± 0.75	35 ± 0.89	19 ± 0.80	27 ± 0.39	11 ± 0.73	26 ± 0.64	9 ± 0.13	18 ± 0.36
Gentamycin	20 ± 0.71	40 ± 0.33	26 ± 0.15	51 ± 0.72	25 ± 0.93	45 ± 0.11						
Fluconazol							24 ± 0.55	37 ± 0.62	16 ± 0.49	31 ± 0.88	15 ± 0.71	25 ± 0.90

of β increases in the studied complexes, in case of V-complex is ~632 times higher than (UREA), ESAPCr complex is ~2464 times higher than (UREA) and Ni-complex is ~936 times higher than (UREA). Therefore, the studied complexes are an efficacious candidate for NLO materials.

3.2. Antimicrobial activity

The *in vitro* antimicrobial actions of ESAP imine ligand and its complexes against three selected bacteria Escherichia coli (−ve), Bacillus subtilis (+ve) and Staphylococcus aureus (+ve)) and three fungi (Aspergillus flavus, Candida albicans and Trichophyton rubrum), were determined. Any chemotherapeutic agent inhibits the growth of microbes by microstatic mechanisms. All of the compounds showed good biological activity with the micro-organism. On contrasting the biological wares of the imine ligand and its complexes with those of a standard bactericide and fungicide, it was obvious that the complexes had conservative activity as matched with the standard, but all the complexes were more active than free ligand. The higher inhibition zone of the transition metal complexes than those of the ligand can be indicated based on the Overtone notion and the chelation theory. Upon chelation, the polarity of the metal ion is decreased to a great extent as the overlap of the ligand orbital and the fractional participating of the positive charge of the metal ion with donor groups. Furthermore, it raises the delocalization of the π-electrons over the whole chelating ring and increases the breakthrough of the complexes into lipid membranes and the blocking of the metal attachment locations in the enzymes of micro-organisms (Abdel-Rahman et al., 2015a,b; 2016a,b,c; 2017a,b,c,d,e; Khanam et al., 2015). The conclusions of the investigations account for the antipathogenic manner of the compounds and this efficacy is positively changed on complexation. Data are listed in Table 8 and Figs. 6 and 7. The minimum inhibitory concentration (MIC) was estimated by serial dilution route and reported in Table 9. The ESAPCr complex (2 and 1.5 mg/mL) was found to be highly effective as they exhibit the lowest MIC against Bacillus subtilis bacteria and Aspergillus flavus fungi compared to other compounds, respectively. The antimicrobial studies indicated that all the complexes indicated significantly enhanced antimicrobial activity against microbial strains in comparison to the free ligands. Previous studies elsewhere suggested that chelation tended to make the ligands perform as more powerful and potent bacteriostatic agents (Creaven et al., 2003), thus inhibited the growth of microbe more than the parent ligands did and it is similar with that of this study. It was suspicious that factors such as solubility, conductivity, dipole moment, and cell permeability mechanism influenced by the existence of metal ion might be the possible cause of the increase in activity. The activities of the tested complexes were confirmed by calculating the potency index (Table S4) according to the following relation (Creaven et al., 2003; Abdel-Rahman et al., 2015a,b; 2016a,b,c; 2017b,c,d,e,f,g):

$$\text{Activity index (A)} = \frac{\text{inhibition zone of complex (mm)}}{\text{inhibition zone of standard drug (mm)}} \times 100 \quad (15)$$

Please cite this article in press as: Abdel-Rahman, L.H. et al., Design and nonlinear optical properties (NLO) using DFT approach of new Cr(III), VO(II), and Ni(II) chelates incorporating tri-dentate imine ligand for DNA interaction, antimicrobial, anticancer activities and molecular docking studies. Arabian Journal of Chemistry (2017), http://dx.doi.org/10.1016/j.arabjc.2017.07.007

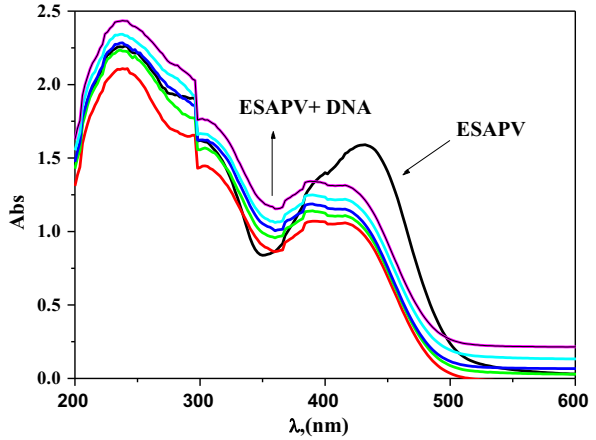

Fig.6 Spectral scans of the interaction of ESAPV complex (10^{-3} mol dm^{-3}) in 0.01 mol dm^{-3} Tris buffer (pH 7.2, 298 K) with CT-DNA (0 −3 0) μM DNA, from top to bottom.

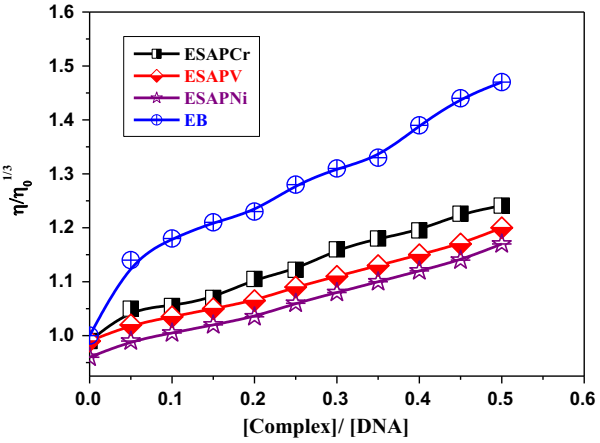

Fig. 7 The effect of increasing concentration of the prepared complexes on the relative viscosities of DNA at (DNA) = 0.5 mM, (complex) and (EB) = 25–250 μM and 298 K.

3.3. DNA binding potency

3.3.1. Electronic spectra of interaction with DNA

Titration with electronic absorption spectroscopy is an active route to check the binding mode of DNA with metal complexes. The spectra were recorded as a function of the addition of the buffer solutions of pretreated CT-DNA to the buffer solutions of the tested complexes. If the interaction mode is intercalation, the orbital of the intercalated ligand can join

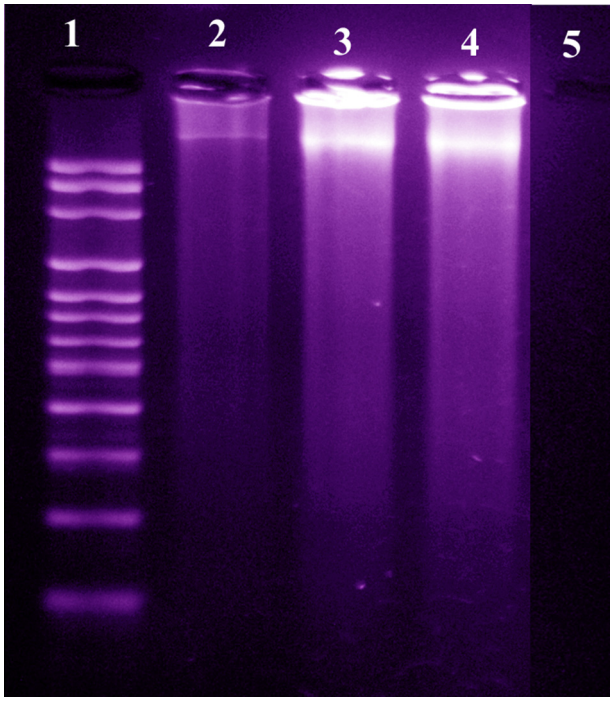

Fig. 8 DNA binding results of the prepared imine complexes based on gel electrophoresis. Lane 1: DNA Ladder, lane 2: ESAPNi + DNA, lane 3: ESAPCr + DNA, lane 4: ESAPV + DNA, lane5: ESAPV complex.

with the orbital of the base pairs, lowering the π–π* transition energy and lead to bathochromism. If the conjunction orbital is partially filled by electrons, it gives rise to reduce the transition probabilities and lead to hypochromism (Abdel-Rahman et al., 2013a,b; 2015a,b; 2016a,b,c; 2017a,b,c,d,e). The electronic absorption spectra of ESNAPV complex in the absence and presence of various concentrations of buffered CT-DNA are given in Fig. 8. Addition of increasing amounts of CT-DNA resulted in a reduction of absorbance for a complex. The spectral parameters and binding constants (K_b) for the DNA interaction with the checked complexes which are calculated using Eq. (12) (cf. Fig. S6), are shown in Table 10. The investigated complexes could bind to DNA mainly *via* an intercalative and replacement modes with the sequence: ESAPCr > ESAPV > ESAPNi complex.

3.3.2. Viscosity measurements

For explaining the interaction nature between the checked complexes and DNA, viscosity measures were executed. Hydrodynamic methods such as viscosity measures which are

Table 9 Minimum inhibition zone (MIC) for antimicrobial assay of the prepared Schiff base and its complexes.

Compounds	Bacteria			Fungi		
	S. aureus	*B. subtilis*	*E. coli*	*A. flavus*	*C. albicans*	*T. rubrum*
ESAP	8	7	7.5	4.5	5.5	6
ESAPV	4	3.5	4.5	2	3.5	2.5
ESAPNi	4	3.5	2.5	2.5	3	3
ESAPCr	3	2	4	1.5	3	2.5

Please cite this article in press as: Abdel-Rahman, L.H. et al., Design and nonlinear optical properties (NLO) using DFT approach of new Cr(III), VO(II), and Ni(II) chelates incorporating tri-dentate imine ligand for DNA interaction, antimicrobial, anticancer activities and molecular docking studies. Arabian Journal of Chemistry (2017), http://dx.doi.org/10.1016/j.arabjc.2017.07.007

Table 10 Spectral parameters for the interaction of the prepared iminecomplexes.

Complex	λ_{max} free (nm)	λ_{max} bound (nm)	Δn	Chromism (%)[a]	Type of Chromism	Binding constant 10^4 (K_b)[b]	ΔG^* (kJ mol^{-1})
ESAPNi	426	418	8	11.2	Hyper	5.10	−26.86
	335	365	30	74.97	Hyper		
ESAPCr	456	435	21	12.65	Hyper	12.44	−29.07
	396	391	5	4.4	Hyper		
ESAPV	433	414	19	17.35	Hyper	6.07	−27.29
	236	237	1	6.58	Hyper		

[a] Chromism (%) = $(Abs_{free} - Abs_{bound})/Abs_{free}$ (Liu et al., 2008; Abdel-Rahman et al., 2015a,b, 2016a,b).
[b] Binding constant K_b = mol^{-1} dm^3.

sensitive to length increment or minimize of DNA are regarded as the most effective methods of studying the binding mode of compounds to DNA in the absence of crystallographic structural data and NMR. For further explaining of the binding mode, viscosity measurements were done. Under suitable conditions, a traditional intercalative mode such as intercalation of drugs like ethidium bromide leads to a obvious increment in the viscosity of DNA solution due to an increment in the segregation of base pairs at the intercalation site and hence an increment in the overall DNA length. On other hand, drug molecules attachment exclusively to the DNA grooves result in less pronounced in DNA solution viscosity (Raja et al., 2012) a partial intercalation of compound may bend the DNA helix, resulting in the reduction of its effective length and, concomitantly, its viscosity (Abdel-Rahman et al., 2016a,b,c; Satyanarayana et al., 1993, Liu et al., 2008). The relative viscosity of DNA solution enhances significantly as the amount of the compound raises, as shown in Fig. 9. This may be due to the admission of the aromatic ring in imine ligand into the DNA base pairs resulting in a crook in the DNA helix, hence, increase in the separation of the base pairs at the intercalation place and increment in DNA molecular length. Moreover, the sequence of the observed increment in the values of viscosity was renovated with the binding affinity to DNA i.e. ESAPCr complex shows the highest binding affinity to DNA and the highest viscosity. Moreover, ESAPCr complex could be bind to DNA via electrostatic binding.

3.3.3. Gel electrophoresis

Agarose gel electrophoresis is used for the DNA binding studies. The prepared imine chelates were studied for their DNA binding activity by agarose gel electrophoresis method (cf. Fig. 10). The gel after electrophoresis clearly showed that the intensity of all the treated DNA samples has partially detracted, possibly because of the interaction with DNA. The partial binding of DNA was observed in the prepared imine chelates . The difference was clarified in the bands of the complexes compared to that of the control DNA. This indicates that the control DNA alone does not show any visible cleavage whereas the complexes show cleavage (Mishra and

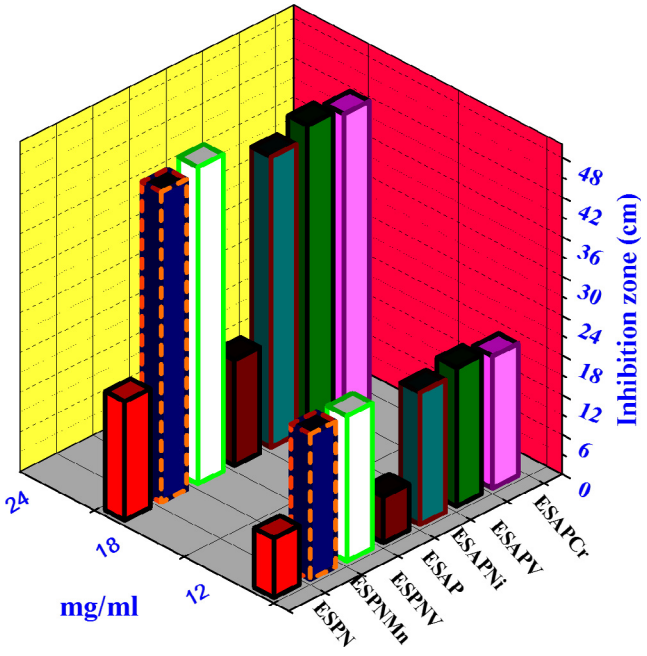

Fig. 9 Histogram showing the comparative antibacterial activities of the prepared compounds (ESAP, ESAP Cr, ESAPNi and ESAPV) against *Bacillus subtilis* bacteria.

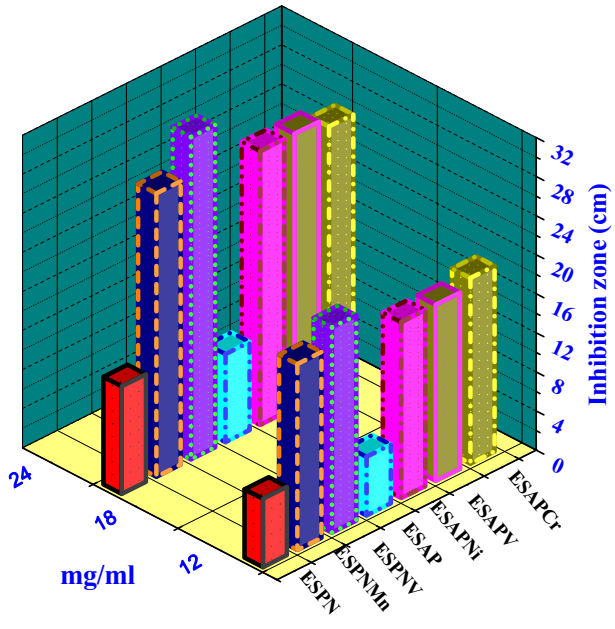

Fig. 10 Histogram showing the comparative antifungal activities of the prepared compounds (ESAP, ESAPCr, ESAPNi and ESAPV) against *C. albicans* fungi.

Please cite this article in press as: Abdel-Rahman, L.H. et al., Design and nonlinear optical properties (NLO) using DFT approach of new Cr(III), VO(II), and Ni(II) chelates incorporating tri-dentate imine ligand for DNA interaction, antimicrobial, anticancer activities and molecular docking studies. Arabian Journal of Chemistry (2017), http://dx.doi.org/10.1016/j.arabjc.2017.07.007

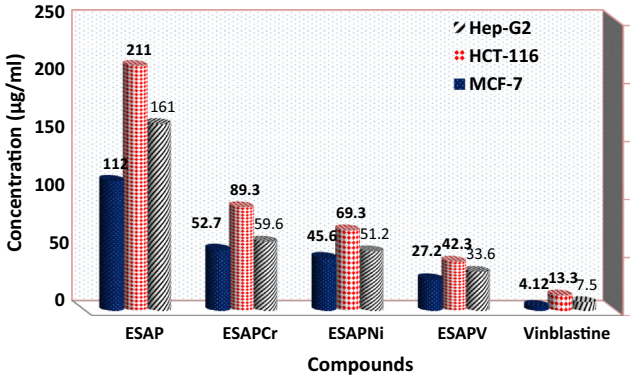

Fig. 11 IC_{50} values of the ESAP imine ligand and its complexes against human colon carcinoma cells (HCT-116 cell line), breast carcinoma cells (MCF-7 cell line) and hepatic cellular carcinoma cells (HepG-2 cell line).

jain, 2012). However, the nature of reactive intermediates involved in the DNA binding by the complexes is not obvious (Yang et al., 1997). These results show that the metal ions play an important role in the interaction with isolated DNA. As the compound was observed to bind with DNA, it can be complemented that the compound minimizes the growth of the pathogenic organism by interaction with genome. The studies reveal that partial binding of DNA was observed by VO(II), Cr(III) and Ni(II) imine complexes.

3.3.4. The proposed mechanism for interaction of the investigated imine complexes with DNA

Correlation between spectral characteristics and hydrodynamic measurements between the investigated complexes and DNA, there are different binding modes can be suggested in our investigation. Complex interacts with DNA most likely through a mode that involves electrostatic or hydrophobic interaction. As stated before, ESAPCr, complex has a replaceable nitrate ligand in solution, which may be replaced with H_2O molecules in the solution (Abdel Rahman et al., 2017c, d). So the complex contains a positive charge in the middle of the Chromium or Mn atoms. This positive charge on the complex ion could easily interaction with negatively charged backbone in phosphate group at the periphery of the double helix CT-DNA *via* electrostatic interaction . Also due to the removal of nitrate ligand from the complex in solution, the investigated complexes will have a flat part in the middle. Therefore, possible interaction of the ESAPCr, complex with DNA could be as follow (cf. Schemes 2a, 2b):

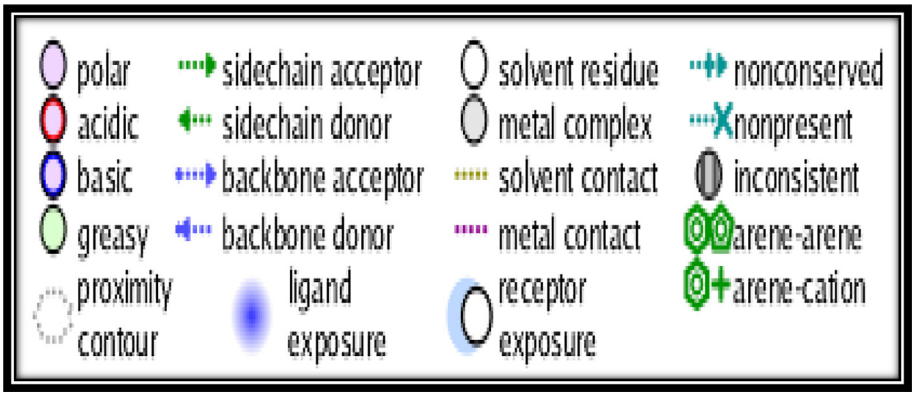

Scheme 3 Representative keys for the type of interactions between the substrate and THR 670.

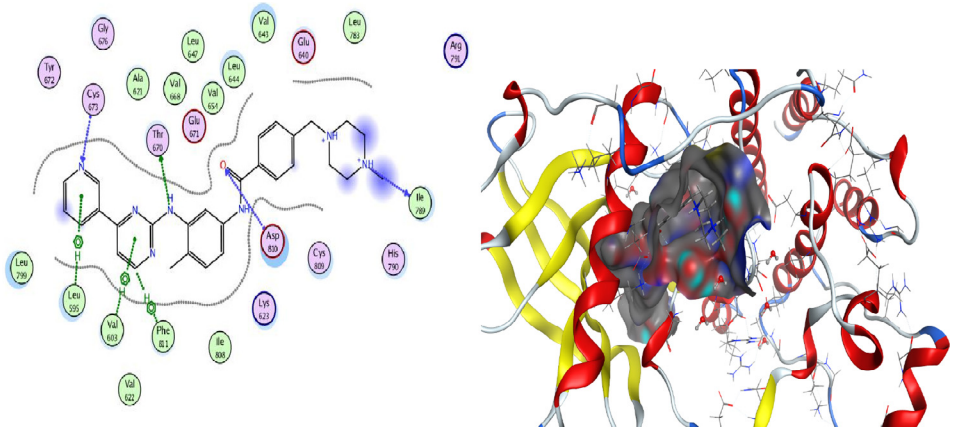

Fig. 12 The binding mode of the native ligand STI with C-kit exhibited one H-bond donor with THR 670 at distance 2.08 and one H-bond donor with ILE 789 at distance 2.19 and one H-bond donor with CYS 673 at distance 2.85 and one H-bond acceptor with HOH 1105 at distance 2.82 its score was − 20.04 kcal mol^{-1} (2D and 3D ligand-receptor interactions).

Please cite this article in press as: Abdel-Rahman, L.H. et al., Design and nonlinear optical properties (NLO) using DFT approach of new Cr(III), VO(II), and Ni(II) chelates incorporating tri-dentate imine ligand for DNA interaction, antimicrobial, anticancer activities and molecular docking studies. Arabian Journal of Chemistry (2017), http://dx.doi.org/10.1016/j.arabjc.2017.07.007

First, interaction of Cr(III) complex with base backbone of DNA or electrostatic interaction of coordination sphere with base pairs of DNA.

Second, insertion of the flat part of the complex between the base pairs and consequently coordination of Cr^{3+} with base pairs of DNA.

3.4. Anticancer activity

The cytotoxic potency of the prepared ESAP imine ligand and its complexes was evaluated against human Colon carcinoma cells (HCT-116 cell line), hepatic cellular carcinoma cells (HepG-2) and breast carcinoma cells (MCF-7 cell line within 0–10 μM concentration range. The IC_{50} values were evaluated for each compound and results are offered in Fig. 11 and Table S5. As shown, most complexes showed manifestly cytotoxic potencies (which are greater than that of ligand) compared to vinblastine standard drug. It seems that changing the complexation locations and the nature of the metal ion has influence on the biological way. Cytotoxicity potency of the complexes may be due to the focal metal atom which was presented by Tweedy's chelation theory (Tweedy, 1964). Cytotoxicity conclusions indicated that all tested complexes (IC_{50} = 42.3–89.3 μg/μl) demonstrated potent cytotoxicity against HCT-116 cancer cells, (IC_{50} = 33.6–59.6 μg/μl) demonstrated potent cytotoxicity against HepG-2 cancer cells and (IC_{50} = 27.2–52.7 μg/μl) demonstrated potent cytotoxicity against MCF-7 cell line. ESAPV complex showed the highest cytotoxicity effect with IC_{50} value of 27.2 μg/μl, followed by ESAPNi complex with IC_{50} value 45.6 μg/μl and then ESAPCr complex with IC_{50} value 52.7 μg/μl in case of all the tested cancer cells. It was spotted also that all complexes are more potent than the free ligand. This showed beneficent of the antitumor potency upon coordination. The refinement of cytotoxic potency may be specified to that the positive charge of the metal increased the acidity of coordinated ligand that gives protons, causing more potent hydrogen bonds which enhanced the biological activity (Feng et al., 2006). It seems that changeable the coordination locations and the nature of the metal ion has a clear impact on the biological manner by modifying the binding ability of DNA (Abdel-Rahman et al., 2015a). Gaetke and Chow had stated that metal has been suggested to smooth oxidative tissue damage through a free-radical mediated trajectory analogous to the Fenton reaction (Gaetke and Chow, 2003).

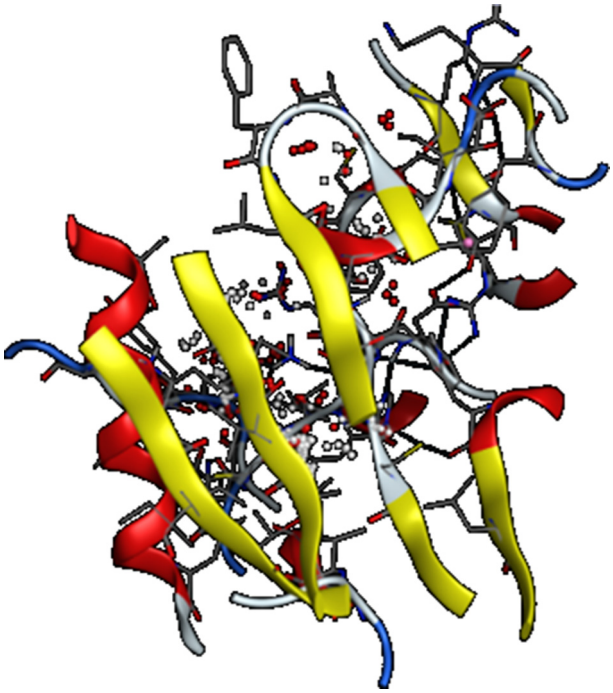

Fig. 14 The proposed binding mode of ESAPV complex docked in the active site of TRK protein; (3D ligand-receptor interactions). The binding mode of ESAPV complex with C-kit receptor exhibited one H-bond acceptor with HOH 1105 at distance 2.14; and one H-bond acceptor with HOH 1106 at distance 3.13 and one H-bond acceptor with HOH 1104 at distance 2.82 and the binding energy is −18.11 kcal/mol.

3.5. Molecular modeling

3.5.1. Molecular modeling: Docking study

The prepared compounds were analyzed for the binding affinity of tyrosine kinases receptor (PDB 1t46) for the purpose of

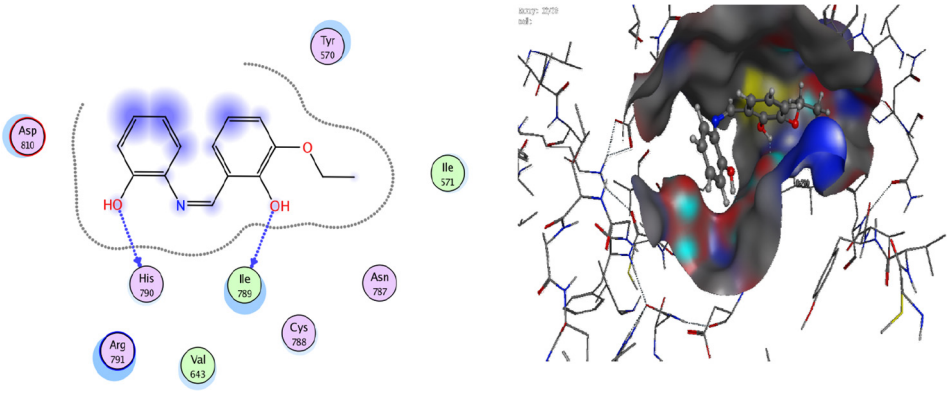

Fig. 13 The proposed binding mode of ESAP ligand docked in the active site of TRK protein; (2D and 3D ligand-receptor interactions). The binding mode of the ligand with C-kit receptor exhibited one H-bond acceptor with Ile789 1105 at distance 2.99; and one hydrophobic interaction with Arg 791 at distance 3.13.

Please cite this article in press as: Abdel-Rahman, L.H. et al., Design and nonlinear optical properties (NLO) using DFT approach of new Cr(III), VO(II), and Ni(II) chelates incorporating tri-dentate imine ligand for DNA interaction, antimicrobial, anticancer activities and molecular docking studies. Arabian Journal of Chemistry (2017), http://dx.doi.org/10.1016/j.arabjc.2017.07.007

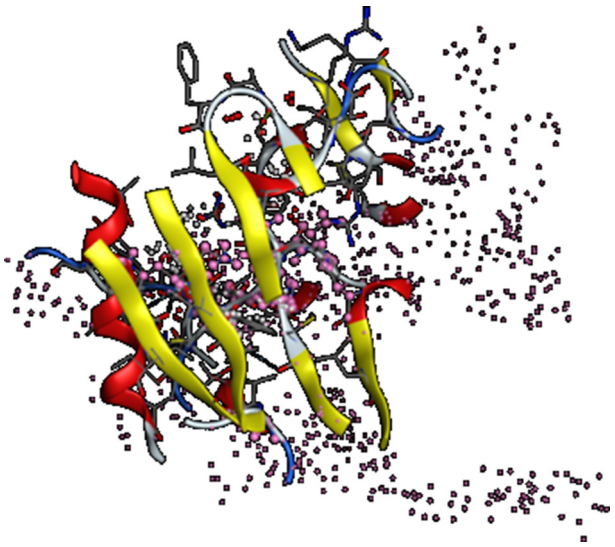

Fig. 15 The proposed binding mode of ESAPCr complex docked in the active site of TRK protein; (3D ligand-receptor interactions). The binding mode of ESAPCr complex with C-kit exhibited one H-bond donor with THR 670 at distance 3.08 and one H-bond donor with ILE 789 at distance 1.99 and one H-bond acceptor with HOH 1105 at distance 2.88 and the binding energy is −17.38 kcal/mol.

Fig. 16 The proposed binding mode of ESAPNi complex docked in the active site of TRK protein; (3D ligand-receptor interactions). The binding mode of ESAPNi complex with C-kit receptor exhibited one H-bond acceptor with Ile789 1106 at distance 1.29; and one hydrophobic interaction with Arg 791 at distance 3.23. H-bond acceptor with HOH 1105 and the binding energy is −11.95 kcal/mol.

both investigate the interaction between studied compounds and c-kit receptor and for lead optimization. Molecular modeling calculation was carried out to investigate the binding free energies of these inhibitor inside the target c-kit kinase receptor. Scheme 3 shows representative keys for the type of interactions between the investigated compounds and THR 670

3.5.2. Validation of the docking performance and accuracy

Docking of the native co-crystallized STI-571 ligand (Imatinib or Gleevec) was used to establish the docking accuracy of the program. The docked ESAP imine ligand was exactly superimposed on the native co-crystallized one with RMSD being 0.40 Å and binding free energies of -20.04 kcal mol^{-1} (cf. Fig. 12). The hydrogen bonds between the docked ESAP imine ligand and the amino acids were the same as those between the amino acid and the native ligand.

3.5.3. The binding affinities of the investigated compounds into c-kit kinase receptor

To compare affinity and to investigate the interaction between the investigated ESAP imine ligand and receptor, molecular docking study was done (cf. Fig. 13). For the docking calculation, firstly, the protein structure (PDB code: 1t46) was separated from the inhibitor and hydrogen atoms were added. The binding free energy, hydrogen bond and RMSD were used to evaluate the binding affinity. All the investigated compounds were docked into the same binding site of the native co-crystallized ligand (cf. Figs. 14–16). The investigated complexes show docking score following sequence ESAPV > ESAPCr > ESAPNi complex (cf. Figs. 14–16).

4. Conclusion

In this study three innovative VO(II), Cr(III) and Ni(II) imine complexes have been synthesized and their structures have been characterized by physicochemical and spectral tools. The obtained results demonstrated that the HNAP imine ligand behaves as dibasic tridentate ONO ligand and coordinates to VO(II), Cr(III) and Ni(II) in 1:1 M ratio. From the analytical and spectral data, it is observed that the complexes adopted octahedral geometry in case of Cr(III), tetrahedral geometry in Ni(II) and distorted square pyramidal geometry in VO(II). The molecular geometry of the studied complexes in the ground state has been calculated by using DFT-B3LYP/GEN level of theory. The optimized structure of the studied complexes are non-linear with the metal ion is not in the same plane as the donating sites. The HOMO-LUMO energy gap calculated at B3LYP/LANL2DZ helped in analyzing the chemical reactivity, hardness, softness, chemical potential and electro negativity. Natural charge distribution of the studied complexes was studied which indicated the electronic charge distribution in the complexes. The calculated dipole moment and first order hyperpolarizability results indicate that the complexes have a reasonable good non-linear optical behavior. The anti-pathogenic screening indicates that these complexes are good antimicrobial agents against different organisms and standards. Moreover, the interaction of the complexes with CT-DNA has been effectively examined and explored by electronic absorption, viscosity measurements and gel electrophoresis. The DNA interaction studies propose the intercalative and replacement modes of interaction. Fur-

Please cite this article in press as: Abdel-Rahman, L.H. et al., Design and nonlinear optical properties (NLO) using DFT approach of new Cr(III), VO(II), and Ni(II) chelates incorporating tri-dentate imine ligand for DNA interaction, antimicrobial, anticancer activities and molecular docking studies. Arabian Journal of Chemistry (2017), http://dx.doi.org/10.1016/j.arabjc.2017.07.007

thermore, the growth inhibitory effect of the prepared compounds was tested on HepG-2, HCT-116 and MCF-7cancer cells. Among these compounds, the compound ESAPV significantly decreases the cell viability time and dose dependently. MOE (molecular modeling environment) determined the binding free energies of these inhibitors into the target c-kit kinase receptor. It was found that the MOE were typically concise with the experimental data. These biological findings from our study would be helpful in perceptive of DNA interaction detected by metal complexes and may lead to develop novel metal based therapeutic drugs.

Acknowledgment

The author are thanks to Mr. Moustafa O. Aboelez, Assistant lecturer of Pharmacy, Faculty of Pharmacy, Sohag University for helping us in doing molecular docking studies.

Appendix A. Supplementary material

Supplementary data associated with this article can be found, in the online version, at http://dx.doi.org/10.1016/j.arabjc.2017.07.007.

References

Abd El-Lateef, Hany M., Abu-Dief, Ahmed M., El-Gendy, Bahaa El-Dien M., 2015a. Investigation of adsorption and inhibition effects of some novel anil compounds towards mild steel in H_2SO_4 solution: Electrochemical and theoretical quantum studies. J. Electroanal. Chem. 758, 135–147.

Abd El-Lateef, Hany, M., Abu-Dief, Ahmed M., Abdel-Rahman, L. H., Sañudo, Eva Carolina, Aliaga-Alcalde, Núria, 2015b. Electrochemical and theoretical quantum approaches on the inhibition of C1018 carbon steel corrosion in acidic medium containing chloride using some newly synthesized phenolic Schiff bases compounds. J. Electroanal. Chem. 743, 120–133.

Abd El-Lateef, Hany, M., Abu-Dief, Ahmed M., Abass, M.A., 2017. Corrosion inhibition of carbon steel pipelines by some novel Schiff base compounds during acidizing treatment of oil wells studied by electrochemical and quantum chemical methods. J. Mol. Struct. 1130, 522–542.

Abdel-Rahman, L.H., El-Khatib, R.M., Nassr, L.A.E., Abu- Dief, A. M., Lashin, F.E., 2013a. Synthesis, physicochemical studies, embryos toxicity and DNA interaction of some new Iron (II) Schiff base amino acid complexes. J. Mol. Struct. 1040, 9–18.

Abdel-Rahman, L.H., El-Khatib, R.M., Nassr, L.A.E., Abu- Dief, A. M., Ismael, M., Seleem, A.A., 2014a. Metal based pharmacologically active agents: synthesis, structural characterization, molecular modeling, CT-DNA binding studies and in vitro antimicrobial screening of iron(II) bromosalicylidene amino acid chelates. Spectrochim. Acta Part A Mol. Biomol. Spectrosc. 117, 366–378.

Abdel-Rahman, L.H., El-Khatib, R.M., Nassr, L.A.E., Abu- Dief, A. M., 2014b. Reactivity trends and kinetic inspection of hydroxide ion attack and DNA interaction on some pharmacologically active agents of Fe(II) amino acid schiff base complexes at different temperatures, 46, 543–553.

Abdel-Rahman, L.H., El-Khatib, R.M., Nassr, L.A.E., Abu- Dief, A. M., 2014c. Kinetic study of the hydroxide ion attack on and DNA interaction with high spin iron(II) Schiff base amino acid chelates baering. ONO Donors 84, 1830–1836.

Abdel-Rahman, L.H., El-Khatib, R.M., Nassr, L.A.E., Abu- Dief, A. M., Lashin, F.E., 2013b. Design, characterization, teratogenicity testing, antibacterial, antifungal and DNA interaction of few high spin Fe (II) Schiff base amino acid complexes. Spectrochim. Acta Part A 111, 266–276.

Abdel-Rahman, L.H., Abu-Dief, A.M., Adam, M.S.S., Hamdan, S.K., 2016d. Some new nano-sized mononuclear Cu(II) Schiff base complexes: design, characterization, molecular modeling and catalytic potentials in benzyl alcohol oxidation. Catal. Lett. 146, 1373–1396.

Abdel-Rahman, L.H., Abu-Dief, A.M., El-Khatib, R.M., Abdel-Fatah, S.M., 2016a. Sonochemical synthesis, DNA binding, antimicrobial evaluation and in vitro anticancer activity of three new nano-sized Cu(II), Co(II) and Ni(II) chelates based on tridentate NOO imine ligands as precursors for metal oxides. J. Photochem. Photobio. B 162, 298–308.

Abdel-Rahman, L.H., Abu-Dief, A.M., Hamdan, S.K., Seleem, A.A., 2015a. Nano structure Iron (II) and Copper (II) Schiff base complexes of a NNO-tridentate ligand as new antibiotic agents: spectral, thermal behaviors and DNA binding ability. Int. J. Nano. Chem. 1 (2), 65–77.

Abdel-Rahman, L.H., Abu-Dief, A.M., Hashem, A.A., Seleem, A.A., 2015b. Recent advances in synthesis, characterization and biological activity of nano sized Schiff Base Amino Acid M(II) complexes. Int. J. Nano. Chem. 1, 79–95.

Abdel-Rahman, L.H., Abu-Dief, A.M., Ismael, M., Mohamed, M.A. A., Hashem, N.A., 2016b. Synthesis, structure elucidation, biological screening, molecular modeling and DNA binding of some Cu (II) chelates incorporating imines derived from amino acids. J. Mol. Struct. 1103, 232–244.

Abdel-Rahman, L.H., Abu-Dief, A.M., Newair, E.F., Hamdan, S.K., 2016c. Some new nano-sized Cr(III), Fe(II), Co(II), and Ni(II) complexes incorporating 2-((E)-(pyridine-2-ylimino)methyl)-napthalen-1-ol ligand: Structural characterization, electrochemical, antioxidant, antimicrobial, antiviral assessment and DNA interaction. J. Photochem. Photobiol. B 160, 18–31.

Abdel-Rahman, L.H., Ismail, N.M., Ismael, M., Abu- Dief, A.M., 2017a. Synthesis, characterization, and biological activity of new mixed ligand transition metal complexes of glutamine, glutaric, and glutamic acid with nitrogen based ligands. Inorg. Nano-Metal Chem. 47, 467–480.

Abdel-Rahman, L.H., Ismail, N.M., Ismael, M., Abu- Dief, A.M., Ahmed, E.A., 2017b. Synthesis, characterization, DFT calculations and biological studies of Mn(II), Fe(II), Co(II) and Cd(II) complexes based on a tetradentate ONNO donor Schiff base ligand. J. Mol. Struct. 1134, 851–862.

Abdel-Rahman, L.H., Abu-Dief, A.M., Aboelez, M.O., Abdel-Mawgoud, Azza A.H., 2017c. DNA interaction, antimicrobial, anticancer activities and molecular docking study of some new VO (II), Cr (III), Mn (II) and Ni (II) mononuclear chelates encompassing quaridentate imine ligand. J. Photochem. Photobiol. B 170, 271–285.

Abdel-Rahman, L.H., Abu-Dief, A.M., Basha, M., Abdel-Mawgoud, Azza A.H., 2017d. Three novel Ni(II), VO(II) and Cr(III) mononuclear complexes encompassing potentially tri -dentate imine ligand: synthesis, structural characterization, DNA interaction, antimicrobial evaluation and anticancer activity. Appl. Organometal. Chem., e3750 http://dx.doi.org/10.1002/aoc.3750.

Abdel Rahman, L.H., Abu-Dief, A.M., Moustafa, H., Hamdan, S.K., 2017e. Ni(II) and Cu(II) complexes with ONNO asymmetric tetradentate Schiff base ligand: synthesis, spectroscopic characterization, theoretical calculations, DNA interaction and antimicrobial studies. Appl. Organometal. Chem. 31, e3555.

Abdel-Rahman, L.H., El-Khatib, R.M., Nassr, L.A.E., Abu-Dief, A. M., 2017f. DNA binding ability mode, spectroscopic studies, hydrophobicity, and in vitro antibacterial evaluation of some new Fe(II) complexes bearing ONO donors amino acid Schiff bases. Arab. J. Chem. 10, S1835–S1846.

Abdel-Rahman, L.H., Abu-Dief, A.M., Abdel-Mawgoud, Azza A.H., 2017g. Development, structural investigation, DNA binding, antimicrobial screening and anticancer activities of two novel

quari-dentate VO (II) and Mn (II) mononuclear complexes. J. King. Saud Uni. Sci. http://dx.doi.org/10.1016/j.jksus.2017.05.011.
Abdel-Rahman, L.H., Abu-Dief, A.M., El-Khatib, R.M., Abdel-Fatah, S.M., 2016e. Some new nano-sized Fe (II), Cd (II) and Zn (II) Schiff base complexes as precursor for metal oxides: Sonochemical synthesis, characterization, DNA interaction, in vitro antimicrobial and anticancer activities. Bioorg. Chem. 69, 140–152.
Abdel-Rahman, L.H., Abu-Dief, A.M., El-Khatib, R.M., Abdel-Fatah, S.M., Seleem, A.A., 2016f. New Cd(II), Mn(II) and Ag(I) Schiff base complexes: synthesis, characterization, DNA binding and antimicrobial activity. Int. J. Nano. Chem. 2 (3), 82–93.
Abu-Dief, A.M., Abdelbaky, M.S.M., García-Granda, S., 2015. Crystal structure of (E)-1-{[(3, 5-dimethylphenyl) imino] methyl} naphthalen-2-ol. Acta Cryst. E71, 496–497.
Abu-Dief, A.M., Mohamed, Ibrahim M.A., 2015. A review on versatile applications of transition metal complexes incorporating Schiff bases. J. Basic Appl. Sci. 4, 119–133.
Abu-Dief, A.M., Nassar, I.F., Elsayed, W.H., 2016. Magnetic $NiFe_2O_4$ nanoparticles: efficient, heterogeneous and reusable catalyst for synthesis of acetylferrocene chalcones and their anti-tumour activity. Appl. Organometal. Chem. 30, 917–923.
Abu-Dief, A.M., Díaz-Torres, R., Sañudo, E.C., Abdel-Rahman, L. H., Alcalde, N.A., 2013. Novel sandwich triple-decker dinuclear NdIII-(bis-N, N0-p-bromo-salicylideneamine-1,2-diaminobenzene) complex. Polyhedron 64, 203–208.
Abu-Dief, A.M., Nassr, L.A.E., 2015. Tailoring, physicochemical characterization, antibacterial and DNA binding mode studies of Cu(II) Schiff bases amino acid bioactive agents incorporating 5-bromo-2-hydroxybenzaldehyde. J. Iran. Chem. Soc. 12, 943–955.
Alaghaz, A.M.A., El-Sayed, B.A., El-Henawy, A.A., Ammar, R.A.A., 2015. J. Mol. Struct. 1087, 60–67.
Anacona, J., Santaella, J., 2013. Spectrochim. Acta A 115, 800.
Armelao, L., Quici, S., Brigelletti, F., Accorsi, G., Bottaroi, G., Cavazzini, M., Tendello, E., 2010. Coord. Chem. Rev. 254, 487–505.
Avci, D., Basoglu, A., Atalay, y., 2010. Ab initio HF and DFT calculations on an organic nonlinear optical material. Struct. Chem. 21 (1), 213–219.
Avci, D., 2011. Second and third-order nonlinear optical properties and molecular parameters of azo chromophores: semiemperical. Spectrochim. Acta A 82, 37–43.
Becke, A.D., 1993. J. Chem. Phys. 98, 5648.
Bradshow, D.S., Andrews, D.L., 2009. J. Nonlinear Opt. Phys. Matter 18, 285–299.
Canali, L., Sherrington, D.C., 1999. Chem. Soc. Rev. 28, 85–93.
Chandra, A.K., Uchimara, T., 2001. Hardness profile: a critical study. J. Phys. Chem. A 105, 3578–3582.
Chemia, D.S., Zysss, J., 1987. Nonlinear Optical Properties of Organic Molecules and Crystals. Academic Press, Orlando, FL.
Chen, X., Yan, F., Wu, M., Tian, H.-B., Li, S.X., Shan, X., Wang, K., Li, Z., Xu, K., 2009. Chem. Phys. Lett. 472, 19.
Creaven, B.S., Duff, B., Egan, D.A., Kavanagh, K., Rosair, G., Thangella, R., Walsh, M., 2010. Inorg. Chim. Acta 363, 4048–4058.
Dyer, J.R., 1965. Applications of Absorption Spectroscopy of Organic Compounds. Prentice-Hall, Englewood Cliffs, NJ, USA.
Feng, G., Mareque-Rivas, J.C., Williams, N.H., 2006. Chem. Commun. 17, 1845–1847.
Frisch, M.J., Trucks, G.W., Schlegel, H. B., Scuseria, G.E., Robb, M. A., Cheeseman, J.R., Montgomery Jr., J.A., Vreven, T., Kudin, K. N., Burant, J.C., Millam, J.M., Iyengar, S.S., Tomasi, J., Barone, V., Mennucci, B., Cossi, M., Scalmani, G., Rega, N., Petersson, G. A., Nakatsuji, H., Hada, M., Ehara, M., Toyota, K., Fukuda, R., Hasegawa, J., Ishida, M., Nakajima, T., Honda, Y., Kitao, O., Nakai, H., Klene, M., Li, X., Knox, J.E., Hratchian, H.P., Cross, J. B., Bakken, V., Adamo, C., Jaramillo, J., Gomperts, R., Stratmann, R.E., Yazyev, O., Austin, A.J., Cammi, C. Pomelli, J.W. Ochterski, P.Y. Ayala, K. Morokuma, G.A. Voth, P. Salvador, R., Dannenberg, J.J., Zakrzewski, V.G., Dapprich, S., Daniels, A.D., Strain, M.C., Farkas, O., Malick, D.K., Rabuck, A.D., Raghavachari, K., Foresman, J.B., Ortiz, J.V., Cui, Q., Baboul, A.G., Clifford, S., Cioslowski, J., Stefanov, B.B., Liu, G., Liashenko, A., Piskorz, P., Komaromi, I., Martin, R.L., Fox, D.J., Keith, T., Al-Laham, M.A., Peng, C.Y., Nanayakkara, A., Challacombe, M., Gill, P.M.W., Johnson, B., Chen, W., Wong, M.W., Gonzalez, C., Pople, J. A., 2009. Gaussian Inc., Wallingford, CT.
Gaetke, L.M., Chow, C.K., 2003. Toxicology 189, 147–163.
Hindo, S.S., Frezza, M., Tomco, D., Heeg, M.J., Hryhorczuk, L., McGarvey, B.R., Dou, Q.P., Verani, C.N., 2009. Metals in anticancer therapy: Copper(II) complexes as inhibitors of the 20S proteasome. Eur. J. Med. Chem. 44, 4353–4361.
Hosseini-Yazdi, S.A., Samadzadeh-Aghdam, P., Mirzaahmadi, A., Khandar, A.A., Mahmoudi, G., Ruck, M., Doert, T., Balula, S.S., Cunha-Silva, L., 2014. Polyhedron 80, 41.
Ismail, T.M.A., Saleh, A.A., El Ghamry, M.A., 2012. Spectrochim. Acta A 86, 276–288.
Lacroix, J., 2001. Eur. J. Inorg. Chem. 2, 339–348.
Lin, X., Doble, D.M.J., Blake, A.J., Harrison, C., Wilson, C., chrder, M.S., 2003. J. Am. Chem. Soc. 125, 9476–9483.
Liu, Y., Mei, W., Lu, J., Zhao, H., He, L., Wu, F., 2008. J. Coord. Chem. 61, 3213–3224.
Marder, S.R., Sohn, J.E., Stucky G.D., 1991. Chemical Perspectives ACS Symposium Series, 455.
Mishra, A.P., Purwar, H., Jain, R.K., 2012. Biointerface Res. 2, 291–299.
Mol, C.D., Dougan, D.R., Schneider, T.R., Skene, R.J., Kraus, M.L., Scheibe, D.N., Snell, G.P., Zou, H., Sang, B.C., Wilson, K.P., 2004. Structural basis for the autoinhibition and STI-571 inhibition of C-Kit tyrosine kinase. J. Biol. Chem. 279, 31655–31663.
Natorajan, S., Shanmugam, G., Martin, S.A., 2008. Cryst. Res. Technal. 43, 561–564.
Raja, D.S., Bhuvanesh, S.P., Natarajan, K., 2012. J. Biol. Inorg. Chem. 17, 223–237.
Reed, A.E., Weinhold, F., 1983. J. Chem. Phys. 78, 4066.
Sarkar, S., Dey, Biswas, S., Bhaumik, B.B., 2007. J. Coor. Chemi. 60 (11), 1143–1156.
Shakir, M., Hanifa, S., Sherwani, M.A., Mohammad, O., Azam, M., Al-Resayes, S.I., 2016. Pharmacophore hybrid approach of new modulated bis-diimine CuII/ZnII complexes based on 5-chloro Isatin Schiff base derivatives: synthesis, spectral studies and comparative biological assessment. J. Photochem. Photobio. B 157, 39–56.
Satyanarayana, S., Dabrowiak, C.J., Chairs, J.B., 1993. Biochemistry 32, 2573–2583.
Schaefer, T., Salman, S.R., Wildman, T.A., Clark, P.D., 1982. Can. J. Chem. 60, 342.
Tweedy, B., 1964. Phytopathology. 55, 910–914.
Wojciechowski, A., Kityk, I.V., Reshak, A.H., Miedzinski, R., Ozga, K., Berdowski, J., Tylczynski, Z., 2010. Mater. Lett. 64, 1957–1959.
Yang, G., Wu, F.Z., Wang, L., NianFi, L., Tina, X., 1997. J. Inorg. Biochem. 66, 141–144.
Khanam, Zakia, Wen, Chew Shwu, Bhat, Irshad Ul Haq, 2015. J. King Saud. Univ. 27, 23–30.
Ziessel, R., 2001. Coord. Chem. Rev. 216, 195.
Zumdahl, S.S., 2000. Chemistry for Chemical and Biological Sciences. University Science Books, Sausalito, CA.

Please cite this article in press as: Abdel-Rahman, L.H. et al., Design and nonlinear optical properties (NLO) using DFT approach of new Cr(III), VO(II), and Ni(II) chelates incorporating tri-dentate imine ligand for DNA interaction, antimicrobial, anticancer activities and molecular docking studies. Arabian Journal of Chemistry (2017), http://dx.doi.org/10.1016/j.arabjc.2017.07.007